UiT
THE ARCTIC
UNIVERSITY
OF NORWAY

Department of Chemistry, Faculty of Science and Technology

Characterization and structural analysis of class D β-lactamases:

variants and mutants of OXA-type carbapenemases

Birgit Helene Berg Nesheim

KJE-3900 Master thesis in Structural Chemistry, May 2016

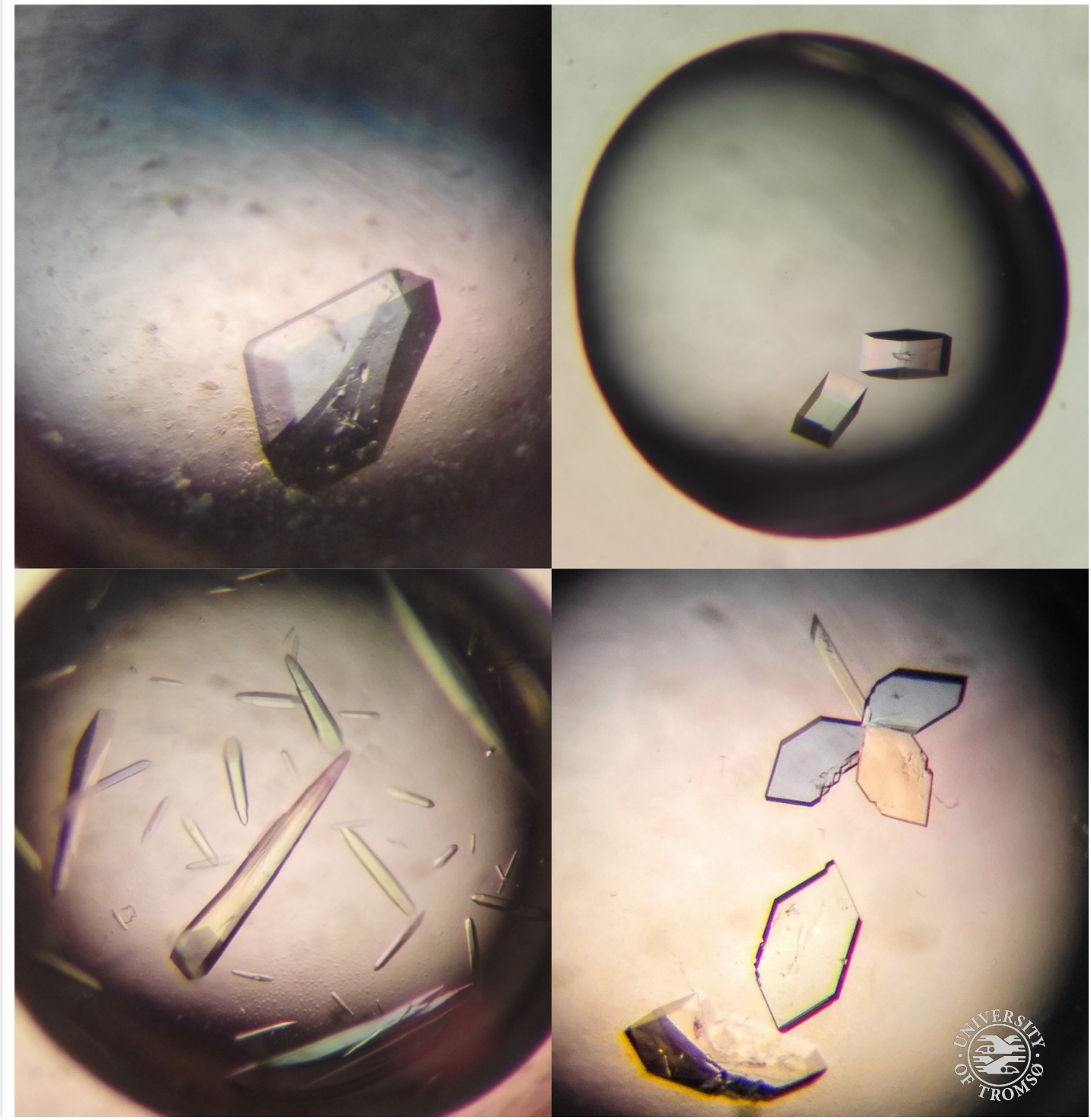

Acknowledgements

First of I would like to thank my supervisor Hanna-Kirsti Leiros for being supportive and patient while guiding me through this year. Secondly I want thank Bjarte Aarmo Lund and Trine Josefine Carlsen for helping me out in the lab and answering all my questions (with great patience) throughout this whole year. Also thank you to rest of the MBL group for helping me when I was stuck.

Abbreviations

A. baumannii	*Acinetobacter baumannii*
Å	Ångstrom
Amp	100 μg/ml Ampicillin
bla	β-lactam resistant gene
Bp	Base pair
BSA	Bovine serum albumin
Cam	34 μg/ml Chloramphenicol
CV	Column volume
Da	Dalton
ddH_2O	Double distilled water
DMSO	Dimethyl sulfoxide
dNTP	Deoxyribonucleotide
E. coli	*Escherichia coli*
EDTA	Ethylene Diamine-tetra-acetic acid
FT	Flow through
Fwd.	Forward
Gent	20 μg/ml Gentamycin
GS	Glycerol stock
Histidine-tag	His-tag
IPTG	Isopropyl-β-D-1-thiogalactopyranoside
K. pneumoniae	*Klebsiella pneumoniae*
LB	Lysogenic broth
mAu	Milli absorbance unit
OD	Optical density
PCR	Polymerase chain reaction
Rev.	Reverse
Rpm	Rounds pr. Minute
SDS	Sodium Dodecyl Sulfate
TB	Terrific broth
TEV	Tobacco etch virus
V	Volt
WT	Wild type
Δε	Extinction coefficient

Abstract

The rise and spread of antibiotic resistant bacteria is posing a serious threat to the global health; antibiotic drugs are rendered ineffective and common infectious diseases become harder or impossible to treat. The β-lactamase enzymes, with their ability to hydrolyze the β-lactam antibiotics, are a major cause of resistant bacteria. The OXA-β-lactamase enzymes are one of the most alarming group, as some members of this group have the ability to hydrolyze and inactivate the carbapenem type β-lactams, which are considered a last resort drug. OXA-23, OXA-24 and OXA-48 are all OXA-enzymes with carbapenem activity. But there is hope on the horizon as new β-lactamase inhibitors are being developed and approved for clinical use. Avibactam is a promising new serine-β-lactamase inhibitor, with the ability to inhibit class A, B and some class C β-lactamases.

This study focused on the three enzymes OXA-23, OXA-24 and OXA-48. It was attempted to clone and express the OXA-23 and OXA-24 proteins from clinical isolates, using a restriction free cloning method. In the end, we were not able to successfully express any of the two proteins.

For the OXA-48 enzyme, the three mutations S118G, R206A and R250A were made in order to study the importance of these enzymes with respect to activity, avibactam binding, and protein dimerization. The S118G and R250A mutations are both in the active site, and enzyme kinetics studies on these mutations showed a significant decrease in the enzyme's ability to hydrolyze carbapenem and penicillin type antibiotics, which gives evidence to the importance of these to residues with respect to the activity of the enzyme. The R206 residue is in a dimer interface interaction, but size exclusion chromatography on the mutant showed that the mutation did not have any effect on the protein dimerization.

Table of Contents

1. Introduction

Since the introduction of penicillin in 1940, modern medicine has relied on the use of antibiotics; they provide a simple solution to infectious diseases, and they are crucial in treatments such as surgery and chemotherapy. The increase in antibiotic resistant bacteria is therefore of great concern to the global health, as it makes infections harder, or impossible to treat and increases the deadliness of common infections. An estimate of 25,000 people dies in Europe each year as a result of infections by multi-drug resistant bacteria, and the 2016 World Economic Forum Global Risks Report listed antibiotic resistance as one of the greatest threats to the global health [1, 2]. Although antibiotic resistance is a natural phenomenon that existed long before the human introduction of antibiotics [3], the widespread use of antibiotics in medicine, agriculture, animal treatment and other areas, puts selective pressure on bacteria to attain resistance genes [4, 5]. The fast spread of resistant genes is, in addition to the vertical transfer of genes between generations of bacteria, caused by horizontal gene transfer between different bacteria; the transfer can occur between different species of bacteria [6].

The β-lactams, which include penicillin, carbapenem, cephalosporin and monobactam, are the most commonly used antibiotics, but the effectiveness of these drugs are decreasing as bacteria confer resistance through the expression of β-lactamase enzymes, which hydrolyzes β-lactams. Structural studies of these β-lactamase enzymes are important in order to understand their mechanism of action, and potentially be able to design β-lactamase inhibitors that can work in conjunction with the β-lactam antibiotics.

1.1 The β-lactam class of antibiotics

The β-lactam group of antibiotics, which include penicillin, carbapenem, cephalosporin and monobactam, all share a β-lactam ring that is crucial to their mode of action. The β-lactams target transpeptidase enzymes, or penicillin binding proteins (PBPs), that synthesize the bacterial cell wall. These enzymes are easily accessible as they are located on the outside of the cytoplasmic membrane of the bacteria, in addition to being specific to bacteria, meaning that the β-lactam antibiotics won't target proteins in the human or animal host.
The cell wall of bacteria consist of a cross linked peptidoglycan layer, which is a repeating chain of alternating *N*-acetyl glucosamine and *N*-acetyl muramic acid residues in equal amounts. The *N*-acetyl muramic acid is modified with a pentapeptide ending in two D-alanine residues, these residues are stereochemically similar to the β-lactam moiety of the β-lactam antibiotics [7]. Transpeptidase enzymes located on the cytoplasmic membrane of the bacteria, catalyzes the formation of a peptide bond between a D-alanine residue on one chain and a diamino pimelic acid (Gram-negative) or L-lysine (Gram-positive) residue on the other chain. β-lactam antibiotics inhibits the transpeptidase enzymes by irreversibly acylating the active site serine residue, which results in the synthesis of a defective cell wall that promotes cell lysis and death [8].

Penicillin was the first antibiotic drug to be discovered by Alexander Fleming in 1928, but it wasn't put in clinical use until 1942 [9]. Since then, a range of different β-lactam antibiotics has been discovered and put to clinical use [10]. The major differences between the types are the spectrum of bacteria of which they are active against. The general structures of the β-lactam groups penicillins, cephalosporins, carbapenems and monobactams are shown in figure 1.1, with the R-group varying between the different types.

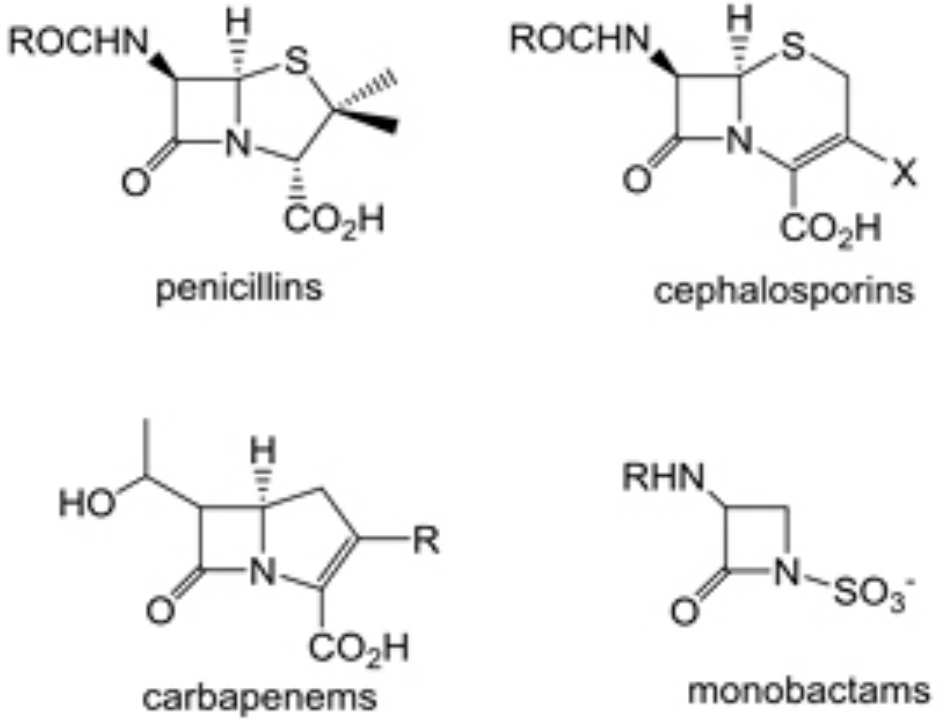

Figure 1.1: The general structure of the β-lactam antibiotics penicillin, cephalosporin, carbapenem and monobactam. Figure from reference [7].

1.2 Antibiotic resistance: the β-lactamase enzymes

Bacteria can obtain resistance to antibiotics through three different mechanisms: reducing the permeability of the cell or increasing the antibiotic efflux, modifications of the antibiotic target or inactivation of the antibiotic itself [11, 12]. The β-lactamase enzymes are an example of the third mechanism, as they work by inactivating β-lactam antibiotics by disrupting the amide bond of the β-lactam ring, thus leaving them inactive. This is the most common mechanism to gain resistance, and the β-lactamase enzymes are widely spread among Gram-positive and Gram-negative bacteria [7]. The β-lactamase genes (*bla* genes*)* are located on both chromosomes and plasmids, and are often associated with mobile genetic elements such as transposons and integrons which facilitates rapid transfer of genetic material between bacteria [7, 13].

The β-lactamases are divided into the four classes A-D based on amino acid sequence [14, 15]. Class B, also called metallo-β-lactamases, have one or two zinc ions in the active site, which are crucial for their activity. Classes A, C (AmpC) and D, or serine-β-lactamases, utilizes an active site serine residue to hydrolyze the β-lactams: the active site serine reacts with a general base to create a nucleophile, which attacks the β-lactam ring to form an acyl-enzyme intermediate, the intermediate is then hydrolyzed by a general base activated water molecule [7, 16]. The general reaction is illustrated in figure 1.2.

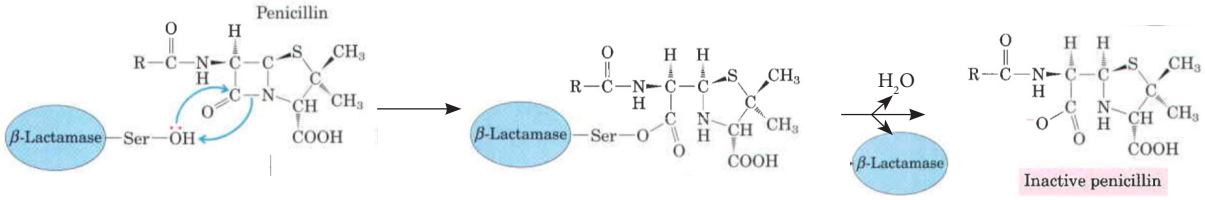

Figure 1.2: The general mode of action of a serine β-lactamase enzyme, with penicillin used as an example β-lactam. Figure from reference [17].

Extended-spectrum β-lactamases (ESBL, classes A and D) have activity against a broad range of β-lactams including penicillins, first- and second generation cephalosporins, third-generation oxyimino cephalosporins and monobactams, and are found in an increasing number of bacteria [18]. The β-lactams cephamycin (similar to cephalosporins), fourth-generation cephalosporins and carbapenems are not affected by ESBLs. The use of carbapenem, which is considered a last resort drug conserved for the treatment of multi-drug resistant (MDR) bacteria, has increased as a result of bacteria carrying ESBL genes [11]. Carbapenemases, which has the ability to hydrolyze a broad range of β-lactams including carbapenems and extended-spectrum cephalosporins, is therefore of great concern. Carbapenemase enzymes are prevalent in both classes A and B, as well as the class D enzymes, or OXA-enzymes. OXA-23, OXA-24 and OXA-48 are all carbapenemases of class D, with a substrate profile including, but not limited to, carbapenem.

1.3 The OXA-type carbapenemases

The OXA name, which is a prefix for oxacillinase, stems from the early enzyme's ability to confer resistance to oxacillin in addition to penicillin [19]. The OXA enzymes were among the first β-lactamases to be discovered, but their substrate profile was mostly limited to penicillins, so their importance was somewhat diminished by other β-lactamases with a broader substrate spectrum. However, from the 1980s, OXA-enzymes with carbapenemase activity started emerging, first in *Acinetobacter baumannii* followed by other species of *Acinetobacter* closely related to *A. baumannii* [19]. In addition, OXA-48-like carbapenemases have migrated to the *Enterobacteriaceae* family of Gram-negative bacteria (i.e. *Klebsiella pneumoniae*), making the OXA-type carbapenemases a serious problem in the field of antibiotic resistance [20]. The level of activity varies among carbapenemases, and sometimes additional resistance mechanisms, like efflux pumps or reduced antibiotic permeability, are required in order for the cell to achieve high levels of resistance [19].

Most of the OXA enzymes are named in the order of which they were described, so similar numbered enzymes are not necessarily structurally similar; the OXA-23 and OXA-24 enzymes only have an amino acid sequence identity of 61%, and the OXA-48 enzyme have sequence identities of 39% and 36% to OXA-23 and OXA-24, respectively [21]. The active site and mode-of-action also varies among the different OXA-enzymes. While OXA-23 and OXA-24 both improve carbapenem affinity by utilizing a hydrophobic bridge spanning the active site [22, 23], the OXA-48 enzyme lacks this bridge, but has a large hydrophobic residue located near the active site, which keeps the carbapenem molecules in a productive conformation (meaning they can be hydrolyzed) [24]. There are however three highly conserved active-site elements that the OXA-enzymes do have in common: this is Ser^{70}-X-X-Lys (X represents a variable residue and Ser^{70} is the active site serine reacting with the β-lactam ring), Ser^{118}-X-Val/Ile (Ser^{118} is one of the residues being mutated in this study) and Lys^{216}-Thr/Ser-Gly (an element that is common in most serine-β-lactamases) [25].

1.3.1 The OXA-23 enzyme

The OXA-23 enzyme was first identified in Edinburgh, UK, in 1985 in an *A. baumannii* isolate. It has also been called ARI-1, an acronym for *Acinetobacter* resistant to imipenem. *A. baumannii* isolates containing the OXA-23 enzyme have since been found in several far-apart countries like China, Brazil and France. The bla_{OXA-23} gene is typically plasmid located, but several bla_{OXA-23}-like genes have been found chromosomally located in isolates of the *Acinetobacter radioresistent* species, which indicates that this may be the enzyme's natural source [26]. The OXA-23 enzyme is reported to have higher activity towards imipenem then it has towards ertapenem, meropenem and doripenem, but the activity is still high enough to give the host strain high level resistance against carbapenems when in combination with additional resistance mechanisms (efflux pumps and reduced permeability) [27].

1.3.2 The OXA-24 enzyme

The OXA-24 enzyme, which was the second OXA enzyme to be discovered after OXA-23, was found in *A. baumannii* isolates in Spain in 1997 [28]. The enzyme is frequently called OXA-40, but will be referred to as OXA-24 throughout this text. The presence of the OXA-24 enzyme is reported to increase the bacterial resistance towards penicillins, carbapenems and cephalosporins, but additional resistance mechanisms are required to reach high levels, as the OXA-24 activity against cephalosporins and carbapenems is generally weak [19].

1.3.3 The OXA-48 enzyme

The OXA-48 enzyme was first discovered in a *Klebsiella pneumoniae* isolate in Istanbul, Turkey in 2001 [29]. The *K. pneumoniae* is a species of the *Enterobacteriaceae* family, so this is a concerning development considering most of the other OXA-type carbapenemases are restricted to the *Acinetobacter* species. Isolates containing these enzymes are widespread in the Middle East, India, in North African counties, and have also been detected in several European countries. Although OXA-48 is most frequently found in *K. pneumoniae*, the enzymes have also been detected in several other species of *Enterobacteriaceae,* including

Escherichia coli, Citrobacter freundii and Escherichia cloacea [20]. The substrate profile of OXA-48 includes penicillins and carbapenems, with high levels hydrolytic activity against penicillins and only weak levels towards carbapenems, but it is reported to have much higher activity towards imipenem then towards meropenem. As with OXA-23 and OXA-24, it has been shown that the presence of OXA-48 in combination with other resistance mechanisms, can result in high levels of carbapenem resistance [19]. The OXA-48 structure is illustrated by a ribbon diagram in figure 1.3, with the active site residues emphasized with yellow sticks.

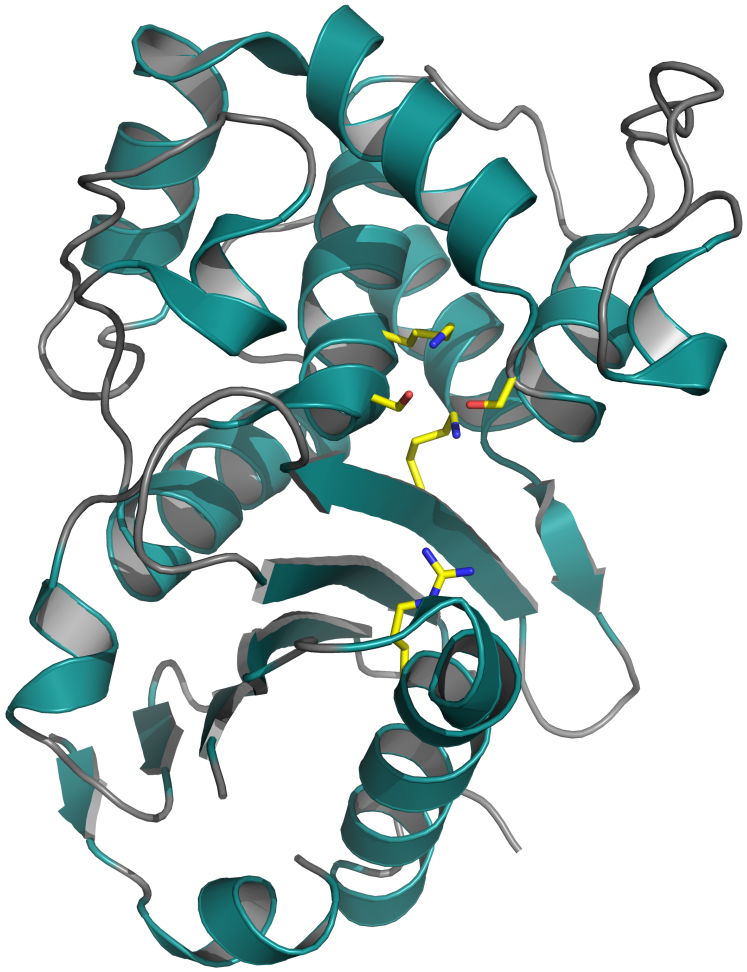

Figure 1.3: A ribbon diagram of the wild type OXA-48. Residues in the active site are shown as yellow sticks. The residues are not numbered, but include Ser70, Lys73, Ser118, Lys208 and Arg250. (PDB ID: 4WMC).

1.3.4 The β-lactamase inhibitor Avibactam and the OXA-48 residues S118 and R250

There are a few β-lactamase inhibitors on the market that work in conjunction with β-lactam antibiotics to overcome β-lactamase resistance. Clavulanate, sulbactam, and tazobactam are commercially available inhibitors that enhance the efficiency of their partner β-lactams [30], but OXA enzymes are not among the β-lactamases being inhibited. Avibactam, a non-β-lactam β-lactamase inhibitor, is currently in clinical development in combination with ceftaroline fosamil and aztreonam [31], and in February 2015 avibactam in combination with ceftazidime (Avycaz) was approved for clinical use in the US [32]. Avibactam has a much broader range of activity then the inhibitors currently on the market, with the ability to inhibit β-lactamase enzymes of class A, C and some class D enzymes, including OXA-23, OXA-24 and OXA-48. It has been shown that avibactam is a covalent, slowly reversible inhibitor [33], with varying acylation rated for the different classes of β-lactamases. In previous studies it has been shown that avibactam shows decent inhibition of OXA-48, with acylation values comparable to that of class C enzymes [34], but the avibactam acylation rates against OXA-23 and OXA-24 was reduced by 5-fold and 28-fold, respectively, when compared to OXA-48. It has been suggested that the reduced acylation rates for these enzymes are a result of the hydrophobic bridge near the active site (that is absent in OXA-48), as it has an impact on the accessibility of the inhibitor to the active site [35]. In addition, the OXA-24 binding pocket is generally more hydrophobic than the OXA-48 binding pocket, which results in fewer polar interactions with avibactam [35]. The molecular structure of avibactam, along with the β-lactamase inhibitors clavulanic acid and tazobactam, is shown in figure 1.4.

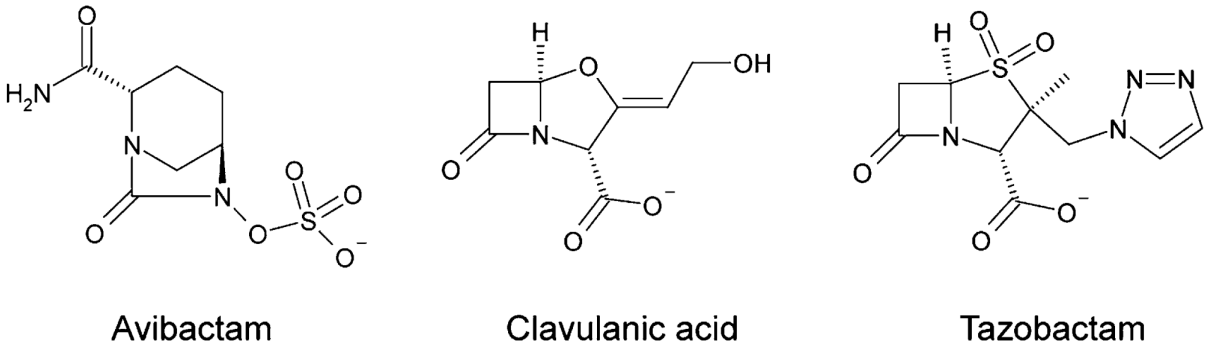

Figure 1.4: The molecular structure of avibactam, clavulanic acid and tazobactam. Avibactam is a non-β-lactam β-lactamase inhibitor, while clavulanic acid and tazobactam has the β-lactam ring present in the structure. Figure from reference [33].

When covalently bound in the active site of OXA-48 to the S70 residue, avibactam is stabilized by polar interactions with several residues as illustrated in figure 1.5. The side chains of the S118 and R250 residues interacts with the sulfamate moiety of avibactam through hydrogen bonds. In this study the S118 and R250 residue will be mutated to glycine and alanine residues, respectively, to study the importance of these residues with respect to avibactam binding and enzyme activity.

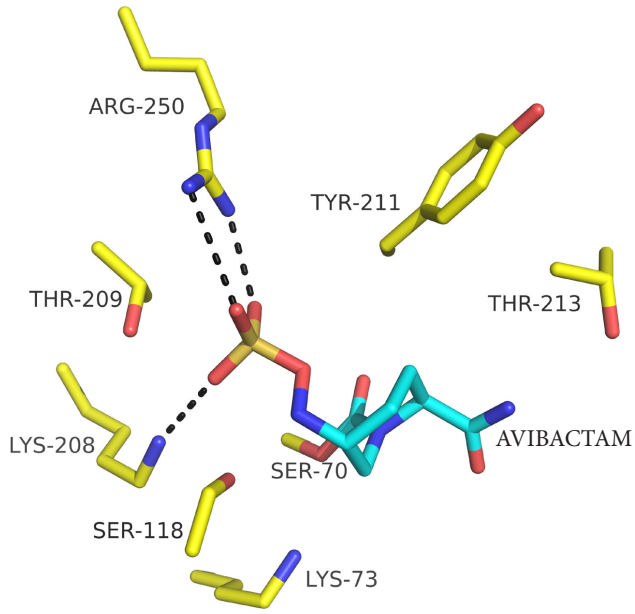

Figure 1.5: Avibactam bound in the active site of OXA-48. OXA-48 residues are represented by yellow sticks, while the avibactam molecule is represented by blue colored sticks. (PBD ID: 4WMC).

1.3.5 The OXA-48 protein as a dimer, and the R206 residue

The OXA-48 enzyme naturally exists as a dimer. The dimer is stabilized by two direct H-bonds between intermolecular β-sheets form each subunit, and water-mediated H-bonds and salt-bridges [24]. In addition to this, the R250 residues of each subunit interact with each other through a chlorine ion as shown in figure 1.6; this residue is to be mutated to an alanine in this study, which can potentially have an effect on the dimerization of the protein, and in turn the activity of the enzyme.

The OXA-10, and its ESBL derivatives also exists as dimers. Several of the derivatives, including OXA-11 and OXA-14, have a glycine-to-aspartate substitution at position 157 that improves the derivatives hydrolysis against ceftazidime, compared to OXA-10 (which is not an ESBL, and does not hydrolyze ceftazidime). The mutation does not affect the active site, but the dimerization of the protein [19, 36], so protein dimerization could have an effect of the hydrolysis activity of the enzyme.

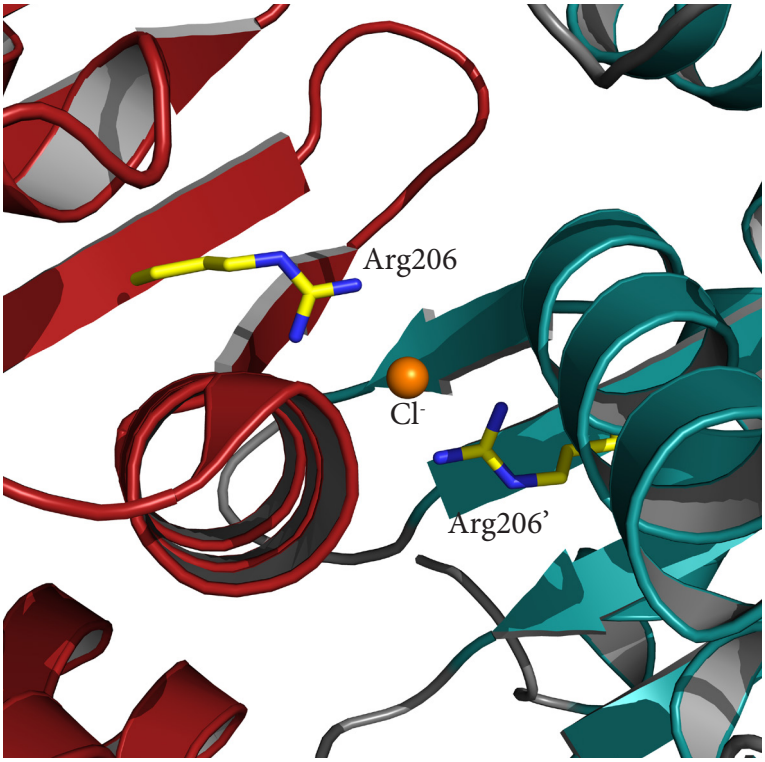

Figure 1.6: The dimer interaction between the two Arg206 residues from each chain, with a chlorine ion between them. PDB ID: 4WMC.

1.4 Enzyme kinetics

Enzyme kinetics is used to study an enzymes activity toward a given substrate. The activity is defined as the enzymes ability to bind to the substrate and subsequently convert the substrate to product; the process is illustrated in equation 1, a model proposed by Leonor Michaelis and Maud Menten in 1913 [37]. The enzyme catalyzes the conversion of substrate to product in a two-step process, where each step has an individual rate-constant. The substrate and enzyme first combine to give the enzyme-substrate (ES) complex through a reversible reaction. The substrate is transformed to product in the second step, and the rate-constant k_{cat} gives the maximum number of substrate molecules converted to product molecules per enzyme per unit of time [37, 38].

(1) $$E + S \overset{K_d}{\Longleftrightarrow} ES \overset{k_{cat}}{\Longleftrightarrow} E + P$$

When substrate concentrations are much higher than enzyme concentrations, the maximum rate, V_{max}, is observed. In this state, V_{max} is constant as there are no available free enzymes to bind and convert additional substrate molecules. K_m is a constant that gives the substrate concentration at $V_{max}/2$, and describes the enzymes affinity for the substrate, a lower value indicates a stronger affinity. k_{cat}/K_m is a rate constant used to describe the overall substrate to product conversion, also called the specificity constant. The Michaelis-Menten equation relates the reaction rate (ν) to the substrate concentration ([S]) (equation 2):

(2) $$\nu = \frac{V_{max} \times [S]}{K_m + [S]}$$

2. Materials and methods

Table 2.1: General buffers and solutions used in the cloning and protein expression process.

Solution	**Contents**
LB medium (1,0 L)	10 g peptone/tryptone 5 g yeast extract 10 g NaCl
LB-agar	10 g peptone/tryptone 5 g yeast extract 10 g NaCl 15 g Agar
TBX medium (0,9 L)	10 g peptone/tryptone 5 g yeast extract 4,6 mL 86% glycerol
10× TB salt (1,0 L)	23,1 g KH_2PO_4 125,4 g K_2HPO_4
TB medium (1,0 L)	100 mL 10× TB salt 900 mL TB medium
SOC medium (1,0 L)	5 g Yeast Extract 20 g Tryptone 0,58 g NaCl 0,19 g KCl 10 mM MgCl2 10 mM MgSO4 20 mM Glucose
NZY^+ (1,0 L)	10 g NZ amine (casein hydrolysate) 5 g yeast extract 5 g NaCl 12.5 mM MgCl2 12.5 mM MgSO4 20 mM glucose
1× Sample buffer (10 mL)	1,25 mL 0,5 M TrisHCl pH 6,8 1,15 mL 20% Sodium Dodecyl Sulfate (SDS) 1,0 mL 86% glycerol 0,5 mL 2-mercaptoethanol 0,1 mL 0,1% bromophenol blue
1× Running buffer	25 mM TrisHCl pH 8,0 192 mM glycine 0,1% SDS

2.1 The β-lactamase enzymes OXA-23 and OXA-24

2.1.1 Restriction free cloning of *bla*$_{OXA-23}$ and *bla*$_{OXA-24}$

Primer design for cloning of bla$_{OXA-23}$ *and bla*$_{OXA-24}$

Two different constructs of both the *bla*$_{OXA-23}$ gene and the *bla*$_{OXA-24}$ gene (GenBank: EF016357 and AJ239129, respectively) were to be cloned in a Gateway pDEST-17 vector using a restriction-free cloning method (devised by Bjarte A. Lund et al. [39]); one native construct of each (native OXA-23 and native OXA-24) with an intact signal sequence that sends the produced protein out to the periplasm, and one construct of each where this signal sequence is removed so that the produced protein is kept inside of the bacterial cell after translation, but with an additional hexahistidine-tag (His-tag) and tobacco etch virus (TEV)-cleavage site sequence.

The webserver rf-cloning.org [40] was used to design forward (F1) and reverse (R1) primers for all four *bla*$_{OXA}$ constructs – the primers, with complementary regions to both the target gene and the pDEST17 vector, were designed to replace the coupled cell division B gene (*ccd*B) with the *bla*$_{OXA}$-genes, enabling negative selection in the transformation process. The work was done in accordance to previous work on *bla*$_{OXA-48}$ [39].

For the native *bla*$_{OXA}$-genes, the forward (fwd.) primers were designed so that the genes were inserted into the pDEST17 vector downstream of the T7 promoter. The reverse (rev.) primers were designed so that the second insertion site is downstream of the toxic *ccd*B-gene encoded in the vector. With these promoters the 822 base pair (bp) long *bla*$_{OXA-23}$ gene and the 828 bp long *bla*$_{OXA-24}$ gene replaced a 1744 bp long region of the pDEST17 vector. This region included a His-tag, a chloramphenicol resistant gene (*CamR*-gene) and the toxic *ccd*B-gene.

In the two His-tagged *bla*$_{OXA}$ constructs a signal sequence at the N-terminal of the genes were to be removed, hindering the produced protein from being sent out to the periplasma of the bacteria. These genes were to be inserted into the vector after a His-tag encoded in

the vector – the His-tag sequence encodes six histidine residues, which enables a very effective affinity purification step in the protein expression and purification process. A TEV cleavage sequence, which is added to the His-tagged *bla*$_{OXA}$ genes in a separate polymerase chain reaction (PCR) reaction using the TEV-site megaprimer shown in table 2.1, encodes a cleavage site for the TEV protease. This is an enzyme that binds very specifically to the TEV cleavage site, enabling easy removal of the His-tag from the purified protein [41]. TEV-cleavage sites have the general amino-acid sequence of Glu-X_{aa}-X_{aa}-Tyr-X_{aa}-Gln-(Gly/Ser), however Glu-Asn-Leu-Tyr-Phe-Gln-Gly is the most common one [41], and was used in these gene-constructs.

In order to identify the signal sequences on the genes, the SignalP 4.1 Server [42] was used. Submitting the OXA-23 and OXA-24 protein sequence encoded from the *bla*$_{OXA-23}$ and *bla*$_{OXA-24}$ genes into the SignalP program gave high score values for a 22 amino acids long sequence at the N-terminal of the OXA-23 enzyme, and a 20 amino acid long sequence at the N-terminal of the OXA-24 enzyme, indicating the signal sequences. The F1 primer for the *bla*$_{OXA-23}$ construct was thus designed to have the protein translated from residue Asp23, or bp 67 in the gene. The F1 primer for the *bla*$_{OXA-24}$ construct was designed to have the protein translated from residue Ser21, or bp 61 in the gene.

The general process behind the restriction free cloning protocol is illustrated in figure 2.1 (for the native *bla*$_{OXA}$ constructs) and in figure 2.2 (for the truncated, His-tagged *bla*$_{OXA}$ constructs).

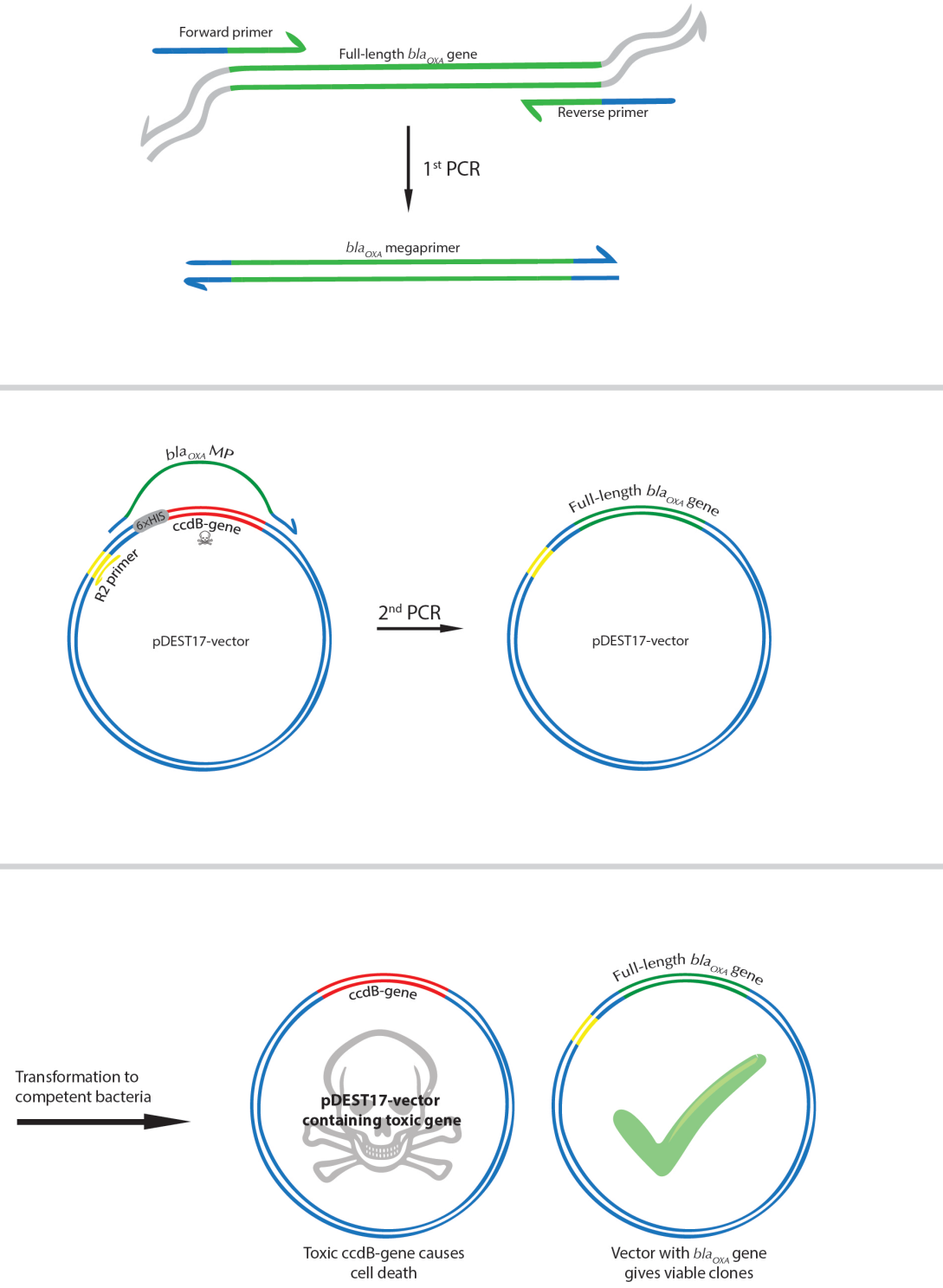

Figure 2.1: The restriction free cloning process of the native *bla*$_{OXA}$ genes. In the first PCR the MPs are created, with the end regions flanking the insertion site of the pDEST17 vector. In the second PCR the MPs are inserted into the pDEST17 vector to replace the toxic *ccdB* gene. In the transformation process, the plasmids that does not have the correct gene are killed by the toxic *ccdB* gene.

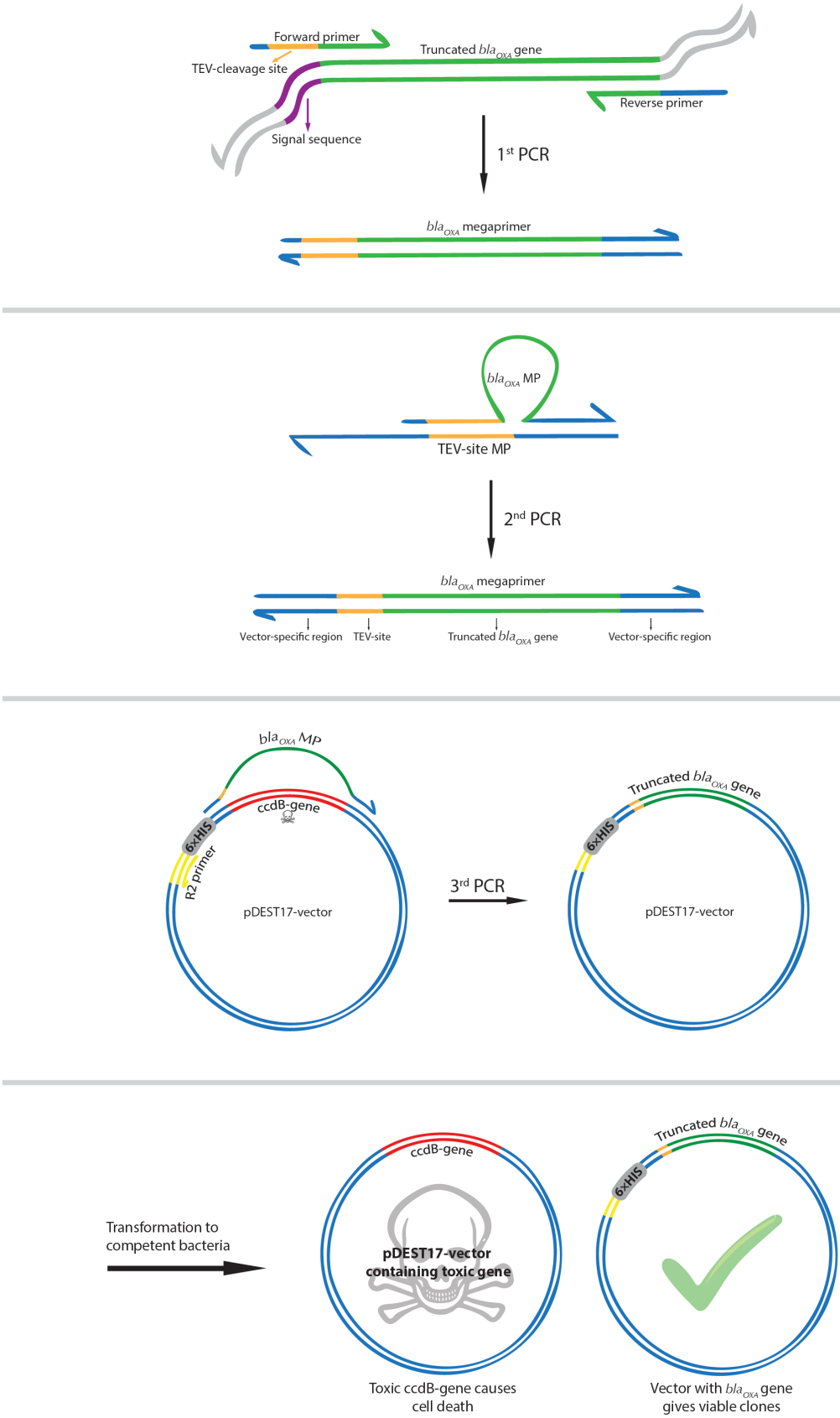

Figure 2.2: The restriction free cloning process of the His-tagged *bla*$_{OXA}$ genes. The general process is the same as for the native genes, but here the His-tag region is not replaced in the vector, and an additional PCR reaction is needed to insert the TEV-site in the MPs.

Table 2.2: Fwd. and rev. primers for native and His-tagged bla_{OXA} genes with underlined letters representing bases complementary to the gene, and normal letters bases complementary to the vector. For the TEV-site MP, the underlined letters represent the TEV-site sequence.

Construct	**Fwd. primer sequence (F1) 5'-3'**	**Rev. primer sequence (R1) 5'-3'**
Native *bla*$_{OXA-23}$	ATAATTTTGTTTAACTTTAAGAAGGAGATA TACATATGAATAAATATTTTACTTGCTATG	GGCTTTGTTAGCAGCCTCGAATCATTAAATA ATATTCAGCTGTTTTAAT
Native *bla*$_{OXA-24}$	ATAATTTTGTTTAACTTTAAGAAGGAGATA TACATATGAAAAAATTTATACTTCCTATAT	GGCTTTGTTAGCAGCCTCGAATCATTAAATG ATTCCAAGATTTTCTAGC
His *bla*$_{OXA-23}$	GTTTGTACGGTGAGAATCTTTATTTTCAGG GTAATTTAATAAATGAAACCCCGAGTC	GGCTTTGTTAGCAGCCTCGAATCATTAAATA ATATTCAGCTGTTTTAAT
His *bla*$_{OXA-24}$	GTTTGTACGGTGAGAATCTTTATTTTCAGG GTTCTATTAAAACTAAATCTGAAGATA	GGCTTTGTTAGCAGCCTCGAATCATTAAATG ATTCCAAGATTTTCTAGC
Other primers used in the cloning process		
TEV-site megaprimer (MP)	ACCATCACCTCGAATCAACAAGTTTGTACGGTGAGAATCTTTATTTTCAG GGTTGATTCGAGGCTGCTAACAAAGCC	
R2-primer	TTCTAGAGGGAAACCGTTGTGGTCT	

PCR amplification of bla$_{OXA}$ megaprimers

100 ng genomic DNA of *bla$_{OXA-23}$* and *bla$_{OXA-24}$* from PCR-positive *Acinetobacter baumannii* isolates by the Norwegian National Advisory Unit on Detection of Antimicrobial Resistance were prepared in a solution with 1xHF Phusion buffer (NEB), 200 μM dNTP, 0,5 μM of both primer F1 and R1, 5% dimethyl sulfoxide (DMSO), 1U Phusion DNA polymerase and dH_2O to a total volume of 50 μL for amplification of the *bla$_{OXA}$* MPs. The *bla$_{OXA-23}$* and *bla$_{OXA-24}$* MPs were then amplified in a PCR reaction: the samples were denatured at 98°C for 30 s before 25 cycles of 8 s denaturation at 98°C, 20 s annealing at 56°C and 15 s elongation at 72°C. The reaction was terminated by 5 min of elongation at 72°C before cooling to 10°C.

DNA analysis of bla$_{OXA-23}$ and bla$_{OXA-24}$ megaprimers by gel electrophoresis

The *bla$_{OXA-23}$* MPs were analyzed by gel electrophoresis – 5 μL of sample was mixed with 1 μl 6x DNA loading buffer (Novagen), and 5 μL of this solution was then loaded into wells in a

1% agarose gel pre-stained with 0,05% (w/v) RedSafe nucleic acid staining solution (ChemBio). 0,5 μL of a 0,1-12 kbp DNA ladder was loaded into one of the wells as a standard and the gel was run at 90 volt (V) for 45 min for separation. The remaining *bla*$_{OXA-23}$ samples were then purified using the NucleoSpin Gel and PCR Clean-up kit (Macherey-Nagel) [43] protocol for PCR clean-up, followed by DNA concentration measurements using a NanoDrop 2000 UV-Vis Spectrophotometer.

For the *bla*$_{OXA-24}$ MPs, the whole 50 μL sample was loaded onto a 1% agarose gel. The reason being that bases 39-49 in the R1 primer has an additional binding site in the interior of the *bla*$_{OXA-24}$ gene, causing the amplification of a shorter gene (283 bases) then desired. To avoid insertion of the shorter gene into the pDEST17 vector in the exponential megapriming PCR (EMP) reaction, the two gene products were separated on an agarose gel and the gene of the correct size was cut out from the gel. 5 μL of 6x DNA loading buffer (Novagen) was mixed with 50 μL of sample, which was then loaded onto a 1% agarose gel and run as previously described. The DNA bands of correct size was identified under UV-light and cut out from the gel. The *bla*$_{OXA-24}$ MPs were purified using the NucleoSpin Gel and PCR Clean-up kit (Macherey-Nagel) protocol for gel extraction, followed by DNA concentration measurements using a NanoDrop 2000 UV-Vis Spectrophotometer at optical density$_{260nm}$ (OD).

Insertion of TEV-cleavage site in His-tagged bla$_{OXA}$ constructs

For the truncated *bla*$_{OXA}$ gene constructs with the His-tags, a TEV-cleavage site had to be inserted between the His-tag and the gene in an additional PCR reaction, using a TEV-site megaprimer constructed by Ph.D. student Bjarte Aarmo Lund. The F1 primers for the His-tagged *bla*$_{OXA}$ constructs have the TEV sequence in them, but in this PCR reaction, the TEV-site megaprimer elongates the 5'-end of the *bla*$_{OXA}$ megaprimers so they have greater overlap with the pDEST17 vector.

For the PCR reaction, two 50 μL solutions containing 1xHF Phusion buffer, 200 μM dNTP, 100 ng TEV MP, 1U Phusion DNA polymerase and 20 μL truncated *bla*$_{OXA-23}$/*bla*$_{OXA-24}$ MP were prepared, and the reactions were denatured at 98°C for 5 min, followed by 10 cycles of 10 s

denaturation at 98°C, 30 s annealing at 56°C and 30s elongation at 72°C. The reaction was terminated by 2 min of elongation at 72°C before cooling to 10°C.

Exponential megapriming PCR (EMP) – insertion of bla_{OXA} gene constructs in pDEST17 vector

Exponential megapriming PCR was performed to insert the bla_{OXA} genes into the pDEST17 vector. In addition to the bla_{OXA} MPs, the R2 primer (table 2.1) complementary to the vector region upstream of the gene insertion site was used to ensure exponential amplification. For each gene – native bla_{OXA-23}/bla_{OXA-24} and His-tagged bla_{OXA-23}/bla_{OXA-24} – a 50 μL reaction containing 1xHF Phusion buffer, 200 μM dNTP, 0.5 mM of each primer R2 and F1, approximately 50 ng pDEST17, 1U Phusion DNA polymerase and approximately 200 ng truncated MP were prepared. The samples were denatured for 30 s at 98°C, followed by 25 cycles of 10 s denaturation at 98°C, 30 s annealing 56°C and 107 s elongation at 72°C before cooling to 10°C.

5 μL of the samples were run on agarose gel electrophoresis using the previously described protocol, and the remaining amount was purified using the NucleoSpin Gel and PCR Clean-up kit (Macherey-Nagel). After purification the EMP products were phosphorylated and ligated by incubating 16.5 μL of PCR product in 1.7 μL 10xT4 DNA ligase buffer (NEB) and 5U T4 polynucleotide kinase at 37°C for 30 min. The samples were then mixed with 6U T4 DNA ligase and incubated at 4°C overnight.

Transformation of pDEST17 bla_{OXA} constructs to E. coli XL1-Blue cells

Each of the EMP products were transformed to chemically competent *E. coli* XL1-Blue cells. 2 μL of DNA product was gently mixed with 50 μL XL1-Blue cells, and the reactions were incubated on ice for 30 min before they were heat-shocked at 42°C for 45s in a water bath. The reactions were kept on ice for approximately 2 min before adding 1 mL SOC medium and incubating at 37°C with 220 rounds per minute (rpm) shaking for 1 hour. 100 μL of each culture was spread on lysogenic broth-agar plates (LB-agar) containing 100 μg/ml ampicillin (Amp) – the rest of the cultures were spun down at 13000 rpm for 1 min, the pellets were re-dissolved in approx. 100 μL supernatant before being spread on LB-agar plates containing 100 μg/ml Amp. The cultures were grown on 37°C overnight.

Amplicon screening of transformed bla_{OXA} constructs

Table 2.3: The fwd. and rev. T7 primers used in the amplicon PCR reaction

Primer	**Primer sequence 5'-3'**
T7 fwd.	TAATACGACTCACTATAGGG
T7 rev.	GCTAGTTATTGCTCAGCGG

For each construct 4 colonies were picked for screening by colony PCR. Each colony was picked with a sterile pipette tip, lightly stroked out on a pre-numbered LB-Agar^{AMP} reference plate before the tip was mixed in a 25 µL solution of 22.5 µL Red Taq, 1 µL T7 primer fwd., 1 µL T7 primer rev. and 0.5 µL double distilled H_2O (ddH_2O). In addition, one negative control with only water, and one positive control with only the plasmid pDEST17 were made. The reference plate was put on 37°C for growth. The reactions were put through the following PCR program: 5 min of denaturation at 98°C, 25 cycles of 30 s denaturation at 98°C, 30 s annealing at 55°C and 30 s elongation at 72°C before being terminated with 7 min of elongation at 72°C. The PCR reactions were analyzed on a gel electrophoresis using the previously described protocol. The amplicon screening showed that the pDEST17 His-tagged *bla_{OXA-24}* construct did not get transformed to the XL1-blue cells, and it was decided to not take the construct any further.

DNA purification and Big-Dye 3.1 sequencing

For the colonies that showed the correctly recombined pDEST17 *bla_{OXA}* product in the colony screening a small amount of bacteria was transferred to 5 mL LB^{AMP} using a sterile inoculation loop and grown overnight at 37°C. This did not include the truncated *bla_{OXA-24}* gene with the His-tag. The pDEST17 *bla_{OXA}* products were isolated from the cells and purified using Wizard *Plus* SV Minipreps DNA Purification System protocol [44], giving 100 µL pure DNA for each construct. The concentration of the purified DNA was measured using a NanoDrop 2000 UV-Vis Spectrophotometer.

The products were prepared for Big Dye 3.1 sequencing [45] by mixing approx. 200 ng of DNA with 1 µL Big Dye 3.1, 4 µL 5x sequencing mix and 1 µL T7 primer fwd./rev. to a final

volume of 20 μL. It was made two parallel reactions for each construct – one with T7 fwd. primer and one with T7 rev. primer. The reactions were denatured at 96°C for 5 min followed by 25 cycles of 10s denaturation at 96°C, 5s annealing at 50°C and 4 min elongation at 60°C. The reactions were terminated by cooling to 10°C.

The reactions were sent in to the sequencing laboratory at the University Hospital of North Norway for Big Dye 3.1 sequencing. The returned sequences were analyzed using the program BLASTN 2.3.1+ [46], by aligning the sequences given by the sequencing laboratory with the *bla*$_{\text{OXA-23}}$ gene and the *bla*$_{\text{OXA-24}}$ gene (GenBank: EF016357 and AJ239129, respectively).

2.1.2 Protein expression of OXA-23 and OXA-24

Transformation and small-scale expression of OXA-23

For the His-tagged and native OXA-23 construct, 1 μL of recombinant plasmid was transformed to competent *E. coli* cell lines BL21(De3)plysS, Rosetta2(De3)plysS and Arctic Express using the previously described protocol for transformation. The plates with BL21 cells and the plates with Rosetta 2 cells contained Amp and chloramphenicol (Cam), and the Arctic Express cells contained Amp and gentamycin (Gent). For the plates with colony growth, amplicon screening was performed followed by analysis by gel electrophoresis.

The colonies with positive results based on the amplicon screening was transferred by an inoculation loop from the reference plate to a 3 mL LB^{AMP} solution for the Arctic Express cells, and a 3 mL $LB^{AMP+CAM}$ solution for the BL21 and Rosetta 2 cells. The pre-cultures were grown on 37°C overnight with 300 rpm shaking.

5 mL LB solutions with the appropriate antibiotics were inoculated with 50 μL pre-culture and grown on 37°C with 220 rpm shaking until log-phase was reached (optical density (OD_{600nm}) values of 0.4-0.9). At log-phase 500 μL of before induction (BFI) culture was collected from each sample for SDS-PAGE analysis. The BFI samples were spun down at 13000 rpm for one minute, the supernatants was discarded, the pellets resuspended in 20 μL sample buffer (SB) and then heated for approx. 5 min at 95°C. In addition to the BFI sample, a glycerol stock (GS) was made by taking out 500 μL of sample and mixing it with 500 μL 86% glycerol. The GS was stored at -80°C for later use.

The rest of the cultures were induced with 0.4 mM Isopropyl-β-D-1-thiogalactopyranoside (IPTG) at 20°C overnight. 500 μL of after induction (AFI) samples were collected from each culture, and treated the same way as the BFI samples. The rest of the induced samples were spun down at 4000 rpm for 15 min, and the pellets were resuspended in 500 μL of Buffer A followed by sonication. 10 μL of cell supernatant (CS) sample was collected from the sonicated samples and mixed with 10 μL of 2xSB before heated at 95°C for 5 min. The rest of the sonicated samples were spun down at 13000 rpm for 1 min and the pellet resuspended

in 500 μL Buffer A. 10 μL of pellet (P) samples were collected for SDS-PAGE analysis from each construct and prepared as described above.

SDS-PAGE analysis of OXA-23 expression

SDS-PAGE was performed on the samples collected to analyze protein expression in the different cell lines. 10 μL of each of the BFI, AFI, CS and P samples were loaded onto 4-20% Mini-PROTEAN TGX Precast Gels (Bio-Rad) together with 7 μL of Precision Plus protein dual color markers (Bio-Rad) as a standard, and ran for 34 min at 200 V in 1x Running buffer. The gel was stained with Simply Blue SafeStain for 10 min before being left in ddH_2O on an orbital shaker overnight to destain.

Large-scale expression of OXA-23 in TB-medium

The cell line Arctic Express was used in large scale expression of the native and His-tagged OXA-23. Pre-cultures were made for each construct by transferring bacteria from the previously made GS solutions to 100 mL LB^{AMP} using an inoculation loop. The pre-cultures were grown on 37°C overnight. There were to be made 4 cultures pr. construct in the large scale production. For each culture, 500 mL of terrific $broth^{AMP+GENT}$ (TB) was inoculated with 5 mL of pre-culture before being grown to log-phase on 37°C with 220 rpm shaking. Before induction at log-phase, 1 mL of BFI sample from each construct was taken and treated as previously described. The cultures were then induced with 0.4 mM of IPTG and put on 20°C with 220 rpm shaking overnight. The OD_{600nm} of the samples were measured, and the equation

(3) $$\frac{OD_{BFI} \times 1000}{OD_{AFI}} = V_{AFI}$$

was used to get the same amount of bacteria in the AFI sample as the BFI sample. SDS-PAGE analysis was run with the AFI and BFI samples.

The cell line BL21(DE3)pRare was also tried as expression host for OXA-23, using the same methods as described above.

Small-scale expression of OXA-24 in 5 mL LB

1 μL of the native OXA-24 construct was transformed to *E. coli* BL21(DE3)pLysS cells by the heat shock protocol described previously. The LB-Agar^{AMP} plates were grown on 37°C overnight, before performing an amplicon screening on the colonies. Three 5 mL LB$^{AMP+CAM}$ pre-cultures were made from three different positive colonies and grown on 37°C overnight. 5 mL LB$^{AMP+CAM}$ solutions were inoculated with 50 μL pre-culture. The OD_{600nm} was measured on the cultures, and they were grown on 37°C with 200 rpm shaking until log-phase was reached. Three GS solutions (stored at -80°C) were collected for later use, before the cultures were induces with 0.4 mM IPTG at 37°C for 2 hours. SDS-PAGE analysis was run.

Large-scale LB and TB expression of OXA-24

A 100 mL LB$^{AMP+CAM}$ pre-culture was made from one of the GS solutions and grown on 37°C overnight. Two samples of 1 L TB$^{AMP+CAM}$, and two samples of 500 mL LB$^{AMP+CAM}$ were inoculated with 10 mL and 5 mL of pre-culture, respectively, before being grown on 37°C with 200 rpm shaking until log-phase was reached. The cultures were induced with 0.4 mM IPTG at 20°C overnight. SDS-PAGE analysis was run with BFI and AFI samples.

Small and large-scale TB expression of OXA-24

The GS solution used in both the LB and TB induction attempts were tested by spreading a small amount on a LB-agar plate and growing it at 37°C overnight. In addition, a new transformation of OXA-24 pDEST17 construct to BL21(DE3)pLysS cells was done. Amplicon screening was performed on both the newly transformed cell colonies and on the colonies from the GS culture. Using the newly transformed cell colonies and the colonies from the GS culture, a small and large scale expression was attempted in six samples of 5 mL LB and five samples of 400 mL TB. The cells from the large scale expression were harvested by centrifuging at 6000 rpm for 40 min. A purification of the protein was attempted as described below. It was also attempted to express the OXA-24 protein in a series of LB volumes: two samples of 5 mL, two samples of 10 mL, two samples of 50 mL, one sample of 100 mL and one sample of 250 mL, before a large scale expression in ten samples of 100 mL LB was attempted.

2.1.3 Ion-exchange purification of native OXA-24

Table 2.4: Buffer used in the purification of OXA-24

Solutions	**Contents**
Buffer A	25 mM Tris pH 7.2
Buffer B	25 mM Bis-Tris-Propane pH 9.5
Buffer C	25 mM Bis-Tris-Propane pH 6.5

Given that the native OXA-24 construct did not have a His-tag, a 70 mL Q Sepharose anion exchange column was used for purification, together with an ÄKTAprime plus (GE Healthcare). The spun down cells were resuspended in 50 mL Buffer A, 15 mg Lysozyme enzyme was added, and the cells were incubated for 15 min. Lysozyme catalyzes the cutting of polysaccharide chains in the cell wall of the bacteria, causing the cell to rupture [38] 0.5 mL $CaCl_2$ was mixed into the sample, and the cells were spun down at 20000 rpm for 45 min. The supernatant containing the proteins were loaded on the 70 mL Q Sepharose column equilibrated on Buffer A. The OXA-24 protein has a theoretical pI of 9.16 as calculated on the ExPASy ProtParam web tool [47], so the column bound contaminants in this step, and the flow through (FT) was collected. 10 μL of the FT was collected and mixed with 10 μL of 2xSB for SDS-PAGE analysis. The column was washed with 5 column volumes (CV) of 1M NaCl. The fractions from the FT were pooled and the pH of the fractions was adjusted to 9.5 by adding a small amount of 1 M NaOH, before diluting the sample twofold with dH_2O.

The column was equilibrated on Buffer B, making the pH of the column 9.5. The sample was loaded on the column, and after collecting the FT, a gradient of 5 CVs (350 mL) from 0 to 100% Buffer C was started to create a pH gradient from 9.5-6.5 – thus eluting the protein and separating it from contaminants. There was a small shift in the fraction numbers on the chromatogram, compared to the fraction number being eluted from the Prime, so a Nitrocefin test was performed to find the fractions containing the OXA-24 enzyme. 980 μL of 50 mM Hepes pH 7.2 was mixed with 10 μL Nitrocefin solved in DMSO (with high enough concentration to give the solution a yellow color), and 10 μL of fraction. The positive fractions changed color from yellow to red. SDS-PAGE analysis was run.

2.2 OXA-48 mutations S118G, R206A and R250A

2.2.1 Site-directed mutagenesis of OXA-48

Primer design for site-directed mutagenesis reaction of OXA-48

To create the three OXA-48 mutations S118G, R206A and R250A, three sets of fwd. and rev. primers were designed based on the sequence of the *bla*$_{OXA-48}$ gene (GenBank: AAP70012) [29]. The program QuikChange Primer Design [48] were used to create the primers showed in table 2.5. In the PCR reaction the primers are complementary to the *bla*$_{OXA-48}$ gene, except for the target codon to be mutated. The target mutations are shown in bold script below.

Table 2.5: The fwd. and rev. primers used in the Mutagenesis reaction for the OXA-48 mutants S118G, R206A and R250A. The target codons for mutation are shown in underlined, bold script.

Construct	**Forward primer (Fwd.)**	**Reverse primer (Rev.)**
S118G	ATAAACAGGCACAAC**TCC**ATATTTCATCGCGGT GATTAGATTATGATCG	CGATCATAATCTAATCACCGCGATGAAATAT**GG A**GTTGTGCCTGTTTAT
R206A	ATCCAGTTTTAGC**CGC**AATAATATAGTCACCATT GGCTTCGGT	ACCGAAGCCAATGGTGACTATATTATT**GCG**GCT AAAACTGGAT
R250A	CTTTTGTGATGGCTTG**GGC**CAGCCCTAAACCTA CCG	CGGATGGTTTAGGGCTG**GCC**CAAGCCATCACA AAAG

Phusion mutagenesis reaction of OXA-48

For the Phusion PCR reaction a construct of *bla*$_{OXA-48}$ in a pDEST17 vector (made by Ph.D. student Bjarte Aarmo Lund) was used along with the QuikChange II Site-Directed Mutagenesis Kit (Agilent). The *bla*$_{OXA-48}$ gene construct had been shortened by 66 bp (22 AA) in the 5'-end; this is a signal sequence that would send the protein out from the cell interior to the periplasma. In addition, the gene construct had been made to have a His-tag and a subsequent TEV-site at the 5'-end.

The reaction was carried out with approximately 50 ng of template in 5 μL of 10x reaction buffer, 1.25 μL (125 ng) fwd. primer, 1.25 μL (125 ng) reverse primer, 1 μL dNTP, and

nuclease-free water to a final volume of 50 μL for each mutant. The mutagenesis reaction and amplification of the DNA was performed with denaturation at 95°C for 30 s followed by 16 cycles of 30 s denaturation at 95°C, 1 min annealing at 55°C and 5.5 min elongation at 68°C. The PCR reactions were then placed on ice for approximately 2 min and spun down on a tabletop centrifuge. To remove the parental DNA from the reaction, 1 μL of 10 Units/μL DpnI restriction enzyme was added to each of the reactions, the DpnI enzyme works by cleaving methylated DNA. The samples were mixed thoroughly and incubated at 37°C for 1 hour for enzymatic digestion of parental DNA.

Transformation of OXA-48 mutants to E. coli XL1-blue cells and amplicon screening of cell colonies

Competent *E. coli* XL1-Blue cells were transformed with the three mutated pDEST17 OXA-48 vectors using the previously described heat shock protocol, but with NZY^+ broth instead of SOC medium. Amplicon screening was performed as previously described, and the constructs were analyzed by gel electrophoresis.

Plasmid prep and Big Dye 3.1 sequencing

For each OXA-48 mutant pDEST17 construct, two 5 mL LB^{AMP} precultures were grown overnight at 37°C at 220 rpm shaking. The plasmids were purified according to the Wizard *Plus* SV Minipreps DNA Purification System protocol [44] followed by a concentration measurement using a NanoDrop 2000 UV-Vis spectrophotometer at OD_{260nm}. The constructs were then prepared for Big Dye 3.1 sequencing [45] by mixing approximately 50 ng of template with 1 μL Big Dye 3.1, 4 μL 5x sequencing mix, 1 μL T7 fwd./rev. primer and dH_2O to a final volume of 20 μL. The reactions were then denatured at 96°C for 5 min followed by 25 cycles of 10 s denaturation at 96°C, 5s annealing at 50°C and 4 min elongation at 60°C before being cooled to 10°C. The samples were sent in to the sequencing laboratory at the University Hospital of North Norway for sequencing, returned sequences were analyzed and confirmed using the program BLASTN 2.3.1+ [46], and viewed in the program SnapGene viewer.

2.2.2 Protein expression of OXA-48 mutants S118G, R206A and R250A

Small scale protein expression of OXA-48 mutants

The pDEST17 OXA-48 mutants were transformed to BL21Star(DE3)pRare cells using the previously described Heat Shock protocol – the LB-agar plates were treated with the antibiotics Amp and Cam. Amplicon screening was performed using the previously described protocol followed by analysis by gel electrophoresis. 5 mL $LB^{AMP+CAM}$ precultures were prepared for each OXA-48 mutant and grown at 37°C overnight. A 5 mL $LB^{AMP+CAM}$ solution was inoculated with 50 μL preculture and grown at 37°C with 220 rpm shaking until log-phase was reached (OD_{600} = 0.4-0.9). GS solutions were collected which were stored at -80°C for later use. The samples were then induced with 0.4 mM IPTG at 37°C for 2 hours. SDS-PAGE gel electrophoresis was run with the BFI and AFI samples.

Large scale protein expression of OXA-48 mutants S118G, R206A and R250A

Three 100 mL $LB^{AMP+CAM}$ precultures were made from the S118G, R206A and R250A GS solutions and grown at 37°C overnight. For each mutant, 2 samples of 1 L $TB^{AMP+CAM}$ medium was inoculated with 10 mL of preculture and grown at 37°C with 220 rpm shaking. OD_{600} was measured regularly until log-phase was reached. At log-phase the samples were induced with 0.4 mM IPTG at 20°C overnight. SDS-PAGE analysis was run previously described.
The cells were harvested with 40 min of centrifuging at 6000 rpm.

2.2.3 Immobilized metal ion affinity chromatography (IMAC) purification of OXA-48 mutants S118G, R206A and R250A

Table 2.6: Buffers used in the purification process of OXA-48 mutants.

Solutions	**Contents**
Buffer D	50 mM HepesHCl pH 7.2 50 mM K_2SO_4
Buffer E	50 mM HepesHCl pH 7.2 50 mM K_2SO_4 500 mM Imidazole
Buffer F (1.0 L)	50 mM HepesHCl pH 7.2 50 mM K_2SO_4 150 mM NaCl 142 μL 2-mercaptoethanol
Buffer G	50 mM HepesHCl pH 7.2 50 mM K_2SO_4
Buffer H	50 mM HepesHCl pH 7.2
Buffer I	50 mM HepesHCl pH 7.2 1M NaCl 50 mM K_2SO_4

Sonication of protein expressed cell samples

The cell pellets from the three spun down cultures were resuspended in approximately 25 mL Buffer D while kept on ice, and one tablet of EDTA-free proteinase inhibitor was mixed with the samples. The samples were then sonicated with 5 s pulse and 9 s break, with 30% amplitude for a total of 45 min sonication. 10 μL of whole cell (WC) samples were collected and mixed with 10 μL of 2x SB before heated at 95°C for 5 min. The sonicated samples were then spun down at 14000 rpm for 40 min, and 10 μL of CS samples were collected and treated the same way as the WC samples. The supernatants were separated from the cell pellets, and collected for purification.

HisTrap purification of OXA-48 mutants, step 1

The OXA-48 mutants were constructed with a His-tag for affinity purification, so a 5 mL HisTrap HP column (GE Healthcare) was used. The column contains nickel ions which have a strong affinity for the histidine tag, making it easy to separate the tagged protein from contaminants [49]. An ÄKTAprime plus (GE Healthcare) machine was used in the purification. The flow rate on the ÄKTAprime plus system was set to 2.5 mL/min, with a pressure limit of

0.5 mPa. The fraction size was 5 mL. The machine was stored on 20% ethanol, so a pump wash was performed first with dH_2O, then with Buffer. The HisTrap column was also stored on ethanol, so it was rinsed with approximately 5 CVs of dH_2O before being equilibrated on Buffer D. The samples were loaded on the column using a 50 mL superloop. After the milli absorbance unit (mAU) had gone below 100, indicating that all FT had been eluted from the column, the column was washed with 5% Buffer E – this was done to elute the weakly bound contaminants from the column. After the mAU had gone down below 100 again, a 70 mL Buffer E gradient was started from 5%-100%, to elute the target protein. Free Imidazole is the elution agent in Buffer E – it acts as a metal ligand that displaces the bound Histidine residues from the Nickel ions on the column [50].

Cleavage of His-tag by TEV protease, and dialysis

SDS-PAGE analysis was run with the WC and CS sample, a fraction of the FT, the contaminant peak, and the elution fractions. The fractions containing the appropriate protein according to MW was pooled to a volume of approximately 45 mL, and a 10 μL before TEV (BTEV) sample was collected for later SDS-PAGE analysis. 4 mL of 7 mg/mL TEV protease was added to the samples for cleavage of the His-tag. A dialysis was performed by transferring the sample to a 10K MW cut-off SnakeSkin (ThermoFisher) in 1 L Buffer F at 4°C overnight.

HisTrap purification of OXA-48 mutants, step 2

Given that the His-tag has been cleaved off, the protein will be eluted in the FT, and His-tagged contaminants and TEV-protease will bind to the column in this step.
10 μL of after TEV (ATEV) sample was collected, before HisTrap purification protocol was performed as described above. The FT was collected, and a 70 mL Buffer E gradient from 0-100% was started to wash the column. SDS-PAGE analysis was performed with the BTEV and ATEV samples, the FT fractions as well as one fraction from the contaminant peak. A SnakeSkin dialysis was performed in 1L Buffer G at 4°C overnight on the S118G and R206A OXA-48 mutants.

Ion exchange purification of OXA-48 R250A mutant

Ion exchange purification was performed on the OXA-48 R250A mutant to separate it from contaminants based on charge. A SnakeSkin dialysis was performed on the pooled fractions from HisTrap step 2 in 1 L of Buffer H (pH 7.2) at 4°C overnight. The 5 mL anion exchange column HiTrap Q HP (GE Healthcare) was used. The OXA-48 R250A mutant has a theoretical pI of 7.24 (calculated using the ExPASy ProtParam [47]), so it will be eluted in the FT using this column. The purification was performed with a flow rate of 2.5 mL/min, a pressure limit of 0.5 mPa and a fraction size of 5 mL, and the protein was eluted with Buffer H. After the FT had been eluted, the contaminants were washed from the column by a Buffer I gradient from 0-100% over 14 CVs. SDS-PAGE analysis was performed with the FT fractions and the contaminant fractions.

Protein concentration

A NanoDrop 2000 spectrophotometer was used to measure the protein absorbance at OD_{280}, and equation (4) was used to convert the absorbance to protein concentration in mg/mL using the values listed in table 2.7.

$$[Protein] = \frac{OD_{280} \times Mw}{extinction\ coeffifient\ (\Delta\varepsilon)} \quad (4)$$

The program ProtParam at ExPASy [47] was used to determine the extinction coefficient and MW of the mutants based on the AA sequence. A 15 mL Amicon Ultra Centrifugal Filter (Millipore) with a 10 kilo Dalton (kDa) cut-off membrane was used to concentrate the proteins. The protein solutions were centrifuged at 4000 rpm until desired concentration (around 15 mg/mL) was reached.

Table 2.7: Mw, Δε and pI values for WT OXA-48 and the three OXA-48 mutants.

OXA-48 construct	**Mw (kDa)**	**Extinction coefficient (Δε)**	**pI**
WT OXA-48	28.147	63940	8.1
OXA-48 S118G	28.117	63940	8.1
OXA-48 R206A	28.062	63940	7.2
OXA-48 R250A	28.062	63940	7.2

2.2.4 Protein crystallography, X-ray data collection and modeling of the three OXA-48 mutants

Table 2.8: Cryoprotectants used in the freezing of OXA-48 mutant crystals

Solution	Contents
Cryo 1	42% PEG 400 0.1 M BistrisPropane pH 9.0
Cryo 2	14% PEG MME5K 0.1 M BisTrisPropane pH 9.0 25% Ethylene glycol

Crystallization of OXA-48 mutants S118G, R206A and R250A

For the S118G mutant, initial trials were set up using a Phoenix DT crystallization robot (Rikagu) with 96-well screens KCSG, StockPEG 17 and Tromsostock 41 (designed by researcher Kenneth Johnson, Norstruct UiT). The screens are made to cover a large area of crystallization conditions, to find one or a few conditions to further optimize. The sitting-drop method was used [51], with 60 μL reservoir solution and a total drop size of 1 μL with 1:1 ratio between protein and reservoir solution. Two drops were made per well: one with the original protein concentration (13.9 mg/mL) and one with the concentration diluted two-fold using the flow-through from the concentration process described above. The trial screens were stored at room temperature.

Based on crystals formed in the initial screening, new 24-well screens were set up manually for further crystal optimization for all three OXA-48 mutants. The hanging drop method was used: the drop containing protein and precipitant solution is placed on a glass cover slip, which is used to seal the well containing the reservoir solution. The drop then hangs above the reservoir solution, and the protein/precipitant solution equilibrates with the larger reservoir solution through vapor diffusion, causing protein crystals to grow in the drop [52]. The reservoir volume was 1 mL and the total drop size 2 μL with 1:1 ratio between protein and reservoir solution. The screen was set up with four different conditions over six wells as shown in table 2.9. Two drops pr. well was prepared, one using the proteins at original concentrations and one where the proteins were diluted two-fold as described above. The crystallization screens for the S118G and R206A mutant were stored at room temperature,

while the crystal screens for the R250A mutant was stored at 4°C as an attempt to slow the crystal growth rate.

Table 2.9: Crystallization conditions for the three OXA-48 mutants

Conditions in row A	Conditions in row B	Conditions in row C	Conditions in row D
38-42% PEG 400 0.1 M BisTrisPropane pH 9.0	38-42% PEG 400 0.1 M BisTrisPropane pH 9.5	14-18% PEG MME5K 0.1 M BisTrisPropane pH 9.0	14-18% PEG MME5K 0.1 M BisTrisPropane pH 9.5

Avibactam soaking of OXA-48 S118G mutant

A S118G crystal was to be soaked with the β-lactamase inhibitor Avibactam before x-ray data collection, to potentially gain some insight with regards to the effect of the mutation on the enzyme's Avibactam-affinity. A 150 mM Avibactam solution solved in 100% DMSO was mixed in Cryosolution 2 to a final concentration of 3.75 mM Avibactam. A 1 μL drop was pipetted out on a glass plate, and a crystal mounting loop was used to transfer a crystal (from row C) to the drop. The glass plate was placed in a hanging-drop style above a 1 mL reservoir solution with row C-conditions (table 2.9). The crystal was soaked in Avibactam overnight at room temperature.

Freezing of OXA-48 protein crystals

Two cryoprotectant solutions were prepared (table 2.8) based on the crystallization conditions. Before being frozen in liquid nitrogen, the crystals were cryoprotected; this prevents formation of ice, which damages the crystal lattice. Flash freezing of crystals in liquid nitrogen generally give better diffraction as it increases the molecular order in the crystal, reduces radiation damage in addition to making the water molecules more ordered, and lastly makes it possible to safely transport the crystals to the Synchrotron location [52]. The crystals were collected using a small crystal mounting loop and transferred to a 1 μL drop of cryoprotectant solution – crystals from row A and B were washed in Cryo 1, those from row C and D were washed in Cryo 2. The crystals were then collected in the crystal mounting loop again, before being being flash frozen by dipping the loop in liquid nitrogen. The crystals that were to be sent to a different site for data collection were stored in a liquid-nitrogen-filled insulated container.

X-ray data collection and structure solving of the three OXA-48 mutants

Diffraction data for the three mutants were collected by Ph.D. student Bjarte Aarmo Lund (Norstruct, UiT) at beamline ID23-2 at the European Synchrotron Radiation Facility, Grenoble, France (mutant S118G soaked in Avibactam), and beamline 14.1 at Bessy II, Berlin, Germany (mutants R206A and R250A). The mutant structures were solved by molecular replacement in Phaser crystallographic software [53] with the OXA-48 wildtype (PDB accession number 5DTK [54]) as a search model. The structures were refined using the Phenix software suite [53, 55], with manual rebuilding in Coot [56].

2.2.5 Enzyme Kinetics

Table 2.10: Buffers used in enzyme kinetics

Solution	Contents
Buffer J	100 mM Sodium Phosphate pH 7.0 50 mM $NaHCO_3$ 0.2 mg/mL bovine serum albumin (BSA)
Buffer K	100 mM Sodium Phosphate pH 7.0 50 mM $NaHCO_3$ 0.2 mg/mL BSA 2.5% DMSO

Table 2.11: Extinction coefficients, plate specific extinction coefficients and wavelengths for the β-lactam substrates used in the enzyme kinetics studies.

β-lactam group	Substrate	Extinction coefficient (Δε)	Plate specific extinction coefficient (Δε, OD/μM)	Wavelength (nm)
Penicillin	Ampicillin	-820	0.000716	235
Cephalosporin	Cefepime	-10000	0.003200	260
Carbapenem	Imipenem	-9000	0.004027	300
Cephalosporin/ reporter substrate	Nitrocefin	17400	0.00645	482

Enzyme kinetics studies were performed to test the activity of the mutants compared to the wildtype OXA-48. The substrates listed in table 2.11 was used in the kinetics studies, along with the buffers listed in table 2.10. A SpectraMax spectrophotometer was used to measure the enzymatic hydrolysis of the substrates at their respective wavelengths (listed in table 2.11), and the reactions took place in 96-well Corning UV microplates.

For each of the substrates, a small amount was dissolved in 1 mL of Buffer J. 10 μL of this mix was then added to a UV-cuvette along with 990 μL of Buffer J. The initial optical density (OD) was then measured at the appropriate wavelength, before 5 μL of 10 nM enzyme was added to the cuvette. The absorbance was then measured at regular intervals until it had stabilized at the end OD. Equation (5) was used to calculate the concentration of the substrates.

(5) $$[Substrate] = \frac{(end\ OD - initial\ OD) \times dilution\ factor}{\Delta\varepsilon}$$

A dilution series of 8 dilutions was made for each substrate; with a concentration range based on previously measured K_m values for wild type OXA-48 (measurements done by Ph.D. student Bjarte A. Lund). The ampicillin concentrations ranged from 1500 μM to 12 μM; the Imipenem concentrations ranged from 100 μM to 0.8 μM, and 1200 μM to 9.4 μM when paired with the S118G mutant; the Nitrocefin concentrations ranged from 250 to 1.9 μM.

For each substrate, three parallel reactions were run. The reactions were carried out in the Spectramax with the appropriate wavelength, for 15 min, with reading intervals of 5 s. In each assay well, 50 μL of Buffer J (Buffer K for nitrocefin) was mixed with 40 μL of substrate from the dilution series, to give the concentrations described above. 10 μL of enzyme was then added quickly to the wells with a multi-channel pipette, to a final concentration of 1 nM enzyme in the wells. The readings were started immediately. The software GraphPad Prism 6 [57] was used to analyze the kinetics data.

2.2.6 Size-exclusion chromatography of OXA-48 mutant R206A

Table 2.12: Buffers used in gel filtration of mutant R206A

Solution	Contents
Buffer L	25 mM Tris pH 7.5 50 mM K_2SO_4
Buffer M	2 M NaCl

For the mutant R206A, a size-exclusion chromatography (SEC) column was run to see the effect of the mutation on the dimerization of the protein. The wildtype OXA-48 enzyme naturally exist as a dimer – Arginine residue 206 in both enzymes in the dimer interacts with each other through a chlorine ion (Figure 1.6); the mutation of residue 206 to an alanine could potentially weaken the interaction enough to hinder the dimerization. Through SEC, one can see if the enzyme is eluted as a dimer or a monomer based on the size of the eluted protein. Two gel filtration columns were run: one without NaCl in the elution buffer, and one with 1 M NaCl in the elution buffer.

A HiLoad 16/600 Superdex 75 pg column (GE Healthcare) was used with a ÄKTApurifier (GE Healthcare) chromatograph, the Superdex 75 pg column material is designed to separate molecules between 3 and 70 kDa.The purified R206S protein was diluted to 1.6 mg/mL in Buffer L, before 1 mL was loaded on the column equilibrated on Buffer L. The protein was eluted with Buffer L, at a flow-rate of 1 mL/min. In the second run, the protein was eluted with 50% Buffer L and 50% Buffer M. The column media in SEC consists of a porous matrix of spherical particles; the smaller molecules enters the pores in the elution process, and thus have to take a longer route through the column then the larger molecules [58] – so the larger molecules will be eluted first, and the smaller molecules will have a delay.
Ph.D. Student Bjarte Aarmo Lund ran a column with the standards Carbonic anhydrase (Mw: 29 kDa), Conalbumin (Mw: 75 kDa) and Aldolase (Mw: 158 kDa) for size determination and to correlate Mw with elution volume.

3. Results

3.1 The β-lactamase enzymes OXA-23 and OXA-24

3.1.1 Restriction-free cloning of *bla*$_{OXA-23}$ and *bla*$_{OXA-24}$

Amplification of bla$_{OXA-23}$ *and bla*$_{OXA-24}$ *MPs*

The *bla*$_{OXA-23}$ and *bla*$_{OXA-24}$ MPs were successfully amplified in the PCR reaction, and verified by gel electrophoresis. Table 3.1 shows the size of the *bla*$_{OXA}$ gene constructs and MPs amplified in the PCR reaction. After purification of the *bla*$_{OXA}$ MPs using the NucleoSpin Gel and PCR Clean-up kit (Macherey-Nagel), the concentrations were measured to 47.4 ng/µL for the native *bla*$_{OXA-23}$ MP, 46.6 ng/µL for the His-tagged *bla*$_{OXA-23}$ MP, 28.9 ng/µL for the native *bla*$_{OXA-24}$ MP and 28.8 ng/µL for the His-tagged *bla*$_{OXA-24}$ MP, using a NanoDrop 2000 UV-Vis spectrophotometer at OD_{260nm}.

Table 3.1: The number of bp in the His-tagged and native *bla*$_{OXA-23}$ and *bla*$_{OXA-24}$ genes, and the number of bp in the MPs. The MPs have more bps then their respective gene-construct, because of overlap with the pDEST17 vector at the endings, constructed for insertion of the gene into the pDEST17 vector.

Construct	**Size of gene construct (bp)**	**Size of MP construct (bp)**
Native *bla*$_{OXA-23}$	822	881
His-tagged *bla*$_{OXA-23}$	756	812
Native *bla*$_{OXA-24}$	828	887
His-tagged *bla*$_{OXA-24}$	765	821

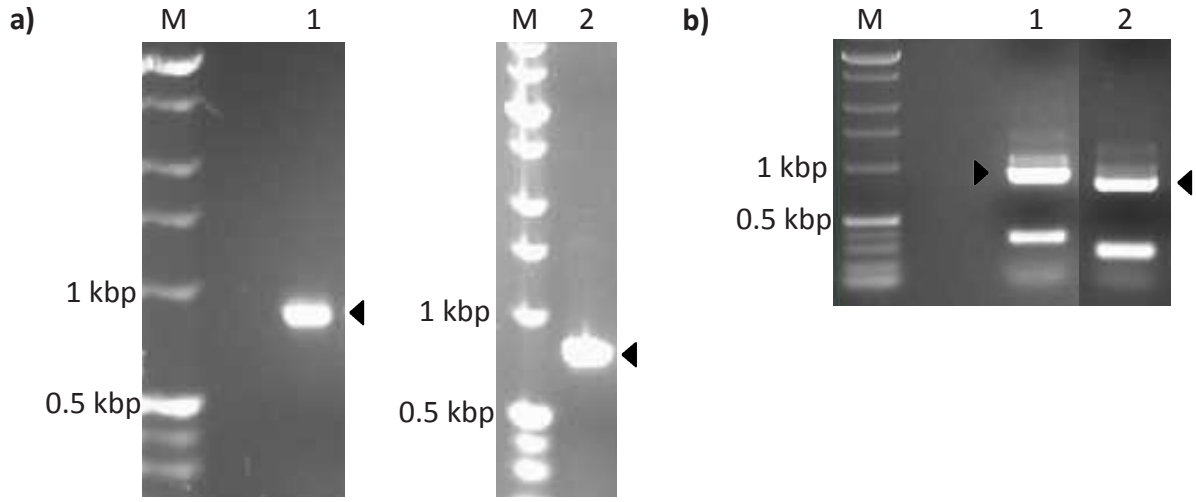

Figure 3.1: Native and His-tagged *bla*$_{OXA-23}$, and native and His-tagged *bla*$_{OXA-24}$ were successfully amplified, constructing the MPs used to insert the gene constructs into the pDEST17 vector in the following EMP reaction. a) Lane 1 shows the PCR product from the native *bla*$_{OXA-23}$ gene amplification and lane 2 shows the PCR product from the His-tagged *bla*$_{OXA-23}$ gene amplification. The M lanes is the Perfect DNA 1 KB ladder, relevant bands are marked on the left side and verifies the size of the PCR products (expected sizes of MPs are shown in table 3.1). **b)** Lane 1 shows the PCR product from the native *bla*$_{OXA-24}$ gene amplification and lane 2 shows the PCR product from the His-tagged *bla*$_{OXA-24}$ gene amplification, the DNA bands of correct size are indicated with an arrow. The bands of smaller size are PCR products which is a result from the binding of the *bla*$_{OXA-24}$ R1 primer to the interior of the *bla*$_{OXA-24}$ gene. The M lanes is the Perfect DNA 1 KB ladder used for size verification.

Insertion of TEV-cleavage site in His-tagged bla$_{OXA}$ constructs

The PCR reaction with the TEV-site MP elongated the His-tagged *bla*$_{OXA}$ MPs with 21 bps, to 812 bps for the *bla*$_{OXA-23}$ construct and 821 bps for the *bla*$_{OXA-24}$ construct. This gives a greater overlap with the pDEST17 vector at the 5'-end of the MPs.

Exponential megapriming PCR (EMP) – insertion of bla$_{OXA}$ gene constructs in pDEST17 vector

The gel electrophoresis showed that all the *bla*$_{OXA}$ constructs got successfully inserted into the pDEST17 vector, as can be seen in figure 3.2. The bands for all four pDEST17 *bla*$_{OXA}$ constructs matched the expected sizes listed in table 3.2, indicating a successful insertion.

Table 3.2: The size of the native pDEST17 vector, as well as the sizes of the pDEST17 vector constructs after the insertion of the *bla*$_{OXA}$ gene constructs.

Construct	**Size of vector construct (bp)**
Native pDEST17	6354
Native *bla*$_{OXA-23}$ pDEST17	5432
His-tagged *bla*$_{OXA-23}$ pDEST17	5441
Native *bla*$_{OXA-24}$ pDEST17	5438
His-tagged *bla*$_{OXA-24}$ pDEST17	5450

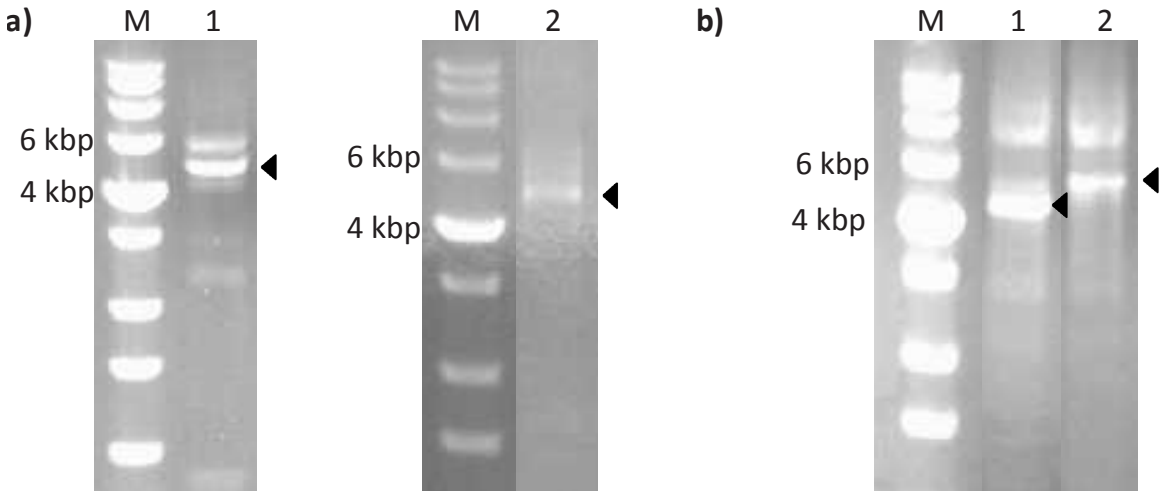

Figure 3.2: Gel electrophoresis analysis of the His-tagged and native *bla*$_{OXA}$ constructs inserted into the pDEST17 vector. The M lanes is the Perfect DNA 1kbp marker, with bands of relevant size marked. **a)** Lane 1 shows the pDEST17 native *bla*$_{OXA-23}$ construct indicated with an arrow, the expected size is listed in table 3.2. The slightly larger band should be the native pDEST17 vector, but these are eliminated in the transformation process by the toxic *ccdB* gene. Lane 2 shows the pDEST17 His-tagged *bla*$_{OXA-23}$ construct at expected size. **b)** Lane 1 shows the pDEST17 native *bla*$_{OXA-24}$ construct, and lane 2 shown the pDEST17 His-tagged *bla*$_{OXA-24}$ construct, both marked with an arrow.

Transformation of pDEST17 bla$_{OXA}$ *constructs to E. coli XL1-Blue cells, and colony screening of transformed constructs*

The transformation resulted in colony growth on all LB-agar plates. Both the His-tagged *bla*$_{OXA}$ constructs failed to transform to the *E. coli* XL1-blue cells, as indicated by the gel electrophoresis of the colony PCR products (figure 3.3). The His-tagged *bla*$_{OXA-24}$ construct was not taken any further at this point, because of time-restraints and a positive result for

the native *bla*$_{OXA-24}$ construct. Both the native *bla*$_{OXA}$ constructs was successfully transformed to the *E. coli* XL1-blue cells, as shown in the gel electrophoresis pictures in figure 3.3.

Table 3.3: The expected sizes of the *bla*$_{OXA}$ gene products after the colony PCR using the T7 fwd. and rev. primers.

Construct	**Size of gene construct from T7 promoter to T7 terminator (bp)**
Native *bla*$_{OXA-23}$	973
His-tagged *bla*$_{OXA-23}$	982
Native *bla*$_{OXA-24}$	979
His-tagged *bla*$_{OXA-24}$	991

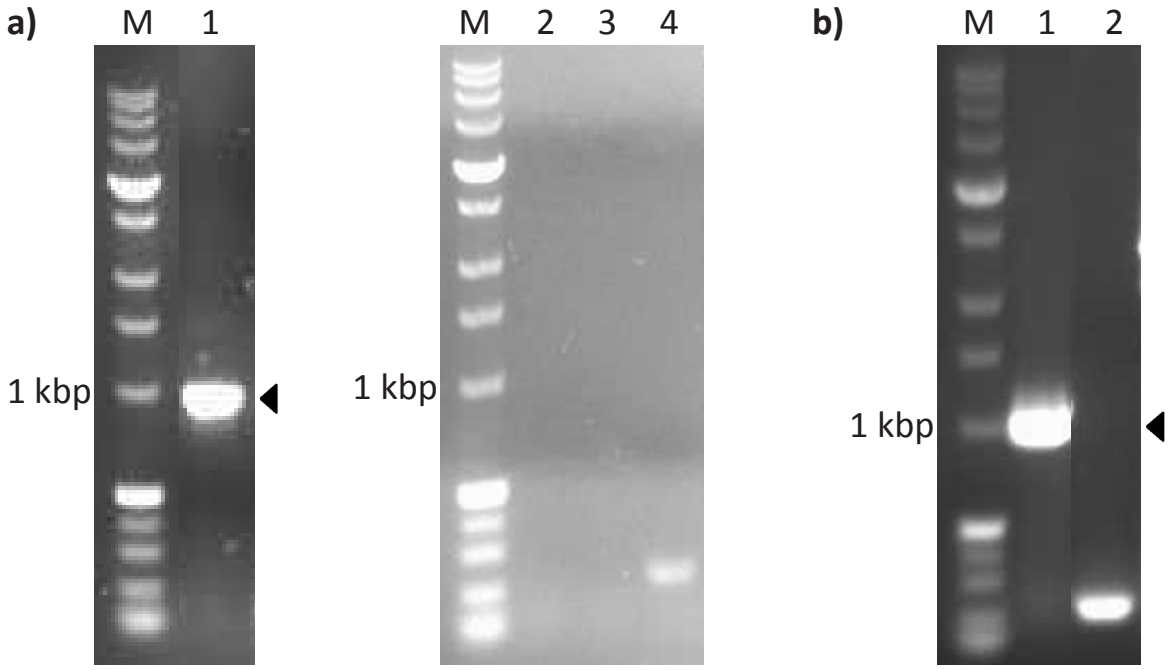

Figure 3.3: The gel results from the colony screening of the pDEST17 *bla*$_{OXA}$ constructs transformed into E. coli XL1-blue cells. T7 primers are used in the colony screening PCR, so the gene is amplified from the T7 promoter to the T7 terminator encoded in the pDEST17 vector. The M lanes is the Perfect DNA 1 kbp marker. **a)** Lane 1 shows the native *bla*$_{OXA-23}$ construct marked with an arrow. Lane 2-4 shows negative screening results for the His-tagged *bla*$_{OXA-23}$ transformation. **b)** Lane 1 shows a positive result for the native *bla*$_{OXA-24}$ construct, the relevant band is marked with an arrow. Lane 2 shows a negative result for the His-tagged *bla*$_{OXA-24}$, indicating that this construct did not get transformed into the XL1-blue cells.

3.1.2 DNA purification and Big-Dye 3.1 sequencing

The His-tagged *bla*$_{OXA-23}$, native *bla*$_{OXA-23}$ and native *bla*$_{OXA-24}$ constructs were purified using the Wizard *Plus* SV Minipreps DNA Purification System protocol, and the concentrations of the purified DNA were measured from 7.3-81.2 ng/μL at 260nm, as listed in table 3.4.

The purified reactions were sent in to the sequencing laboratory at the University Hospital of North Norway for Big Dye 3.1 sequencing. The returned sequences were analyzed using the program BLASTN 2.3.1+ [59] in addition to the program SnapGene Viewer [60].

Table 3.4: The concentrations of the *bla*$_{OXA}$ constructs after the DNA purification.

Construct	**Concentration (ng/μL)**
Native *bla*$_{OXA-23}$	7.3
His-tagged *bla*$_{OXA-23}$	57.9
Native *bla*$_{OXA-24}$	81.2

Sequencing results from the native bla$_{OXA-24}$ *gene*

The native *bla*$_{OXA-24}$ sequence alignment gave identities = 824/830 (99%) and gaps = 2/830 for the T7 fwd. primer sequence, and identities = 825/829 (99%) and gaps = 2/829 for the T7 rev. primer sequence. No mutations were found when viewing the chromatogram in the SnapGene Viewer program, and the errors and gaps could be explained as sequencing errors.

Sequencing results from the His-tagged bla$_{OXA-23}$ *gene*

The His-tagged *bla*$_{OXA-23}$ alignment, when reading from 5' to 3' from the T7 promoter, gave identities = 809/809 (100%) and gaps = 0/809 (0%) when aligning the sequenced gene with the *bla*$_{OXA-23}$ gene including the his-tag and the TEV-site sequence at the 5'-end of the gene. When reading from 3' to 5' from the T7 terminator, it gave identities = 809/809 (100%) and gaps = 0/809 (0%). The entire *bla*$_{OXA-23}$ gene was cloned successfully without any mutations.

There was however found an error around the His-tag region of the sequence. As shown in figure 3.4, a 21 bp long region of the sequence was duplicated right after the His-tag; this

region matches exactly with the 21 bp long region at the 5'-end of the TEV-site MP that does not complement the *bla*$_{OXA-23}$ MP, but is there to elongate the overlap to the pDEST17 vector. Translating the sequenced nucleotide chain with the duplicated sequence, using the ExPASy translate tool [61], showed that the *bla*$_{OXA-23}$ gene is still in the reading-frame, so expressing the gene should still be possible with the error. The His-tag sequence, the TEV-site and the OXA-23 enzyme would still be translated correctly, but with a longer sequence of amino acids between the His-tag and TEV-site sequence.

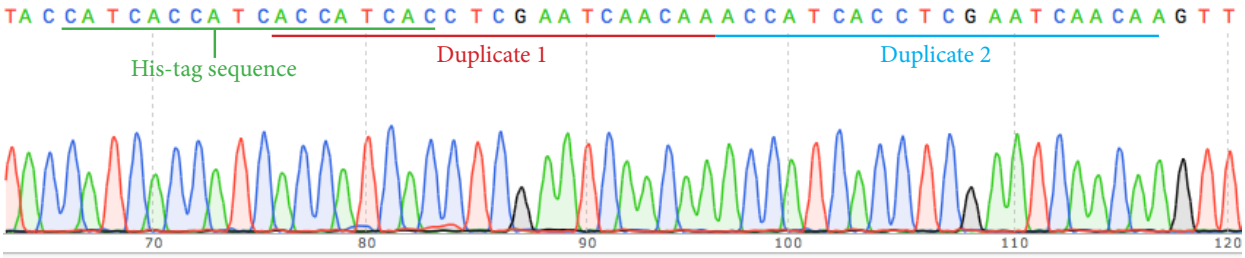

Figure 3.4: Chromatogram from the sequencing of the His-tagged *bla*$_{OXA-23}$ gene showed a duplicated region around the His-tag sequence (underlined in green color). The repeated sequence is underlined in red and blue color.

Sequencing results from the native bla$_{OXA-23}$ *gene*

The native *bla*$_{OXA-23}$ gene was only sequenced from the T7 terminator and backwards, and because of a reading-length shorter than the gene, the *bla*$_{OXA-23}$ cloning was only confirmed from base 139 to 822. The alignment gave identities = 679/684 (99%) and gaps = 0/684 (0%). This confirms that the gene is correctly inserted from base 139 to the end of the gene, and one could assume a correct insertion from base 1 to base 138 as well.

3.1.3 Protein expression of native and His-tagged OXA-23 and native OXA-24

Table 3.5: The expected sizes of the native and His-tagged OXA-23 constructs, and the native OXA-24 construct. The weights are calculated using the ExPASy ProtParam program [47].

Construct	**Molecular weight (kDa)**
Native OXA-23	30.979
His-tagged OXA-23 (without signal sequence)	31.555
Native OXA-24	30.939

Small-scale and large-scale expression of OXA-23

The native and His-tagged OXA-23 construct were transformed into the *E. coli* cell lines Arctic Express, Rosetta2(DE3)plysS and BL21(DE3)plysS. The native OXA-23 transformation to Rosetta2(DE3)plysS and BL21(DE3)plysS did not yield any colonies on the LB-agar$^{AMP+CAM}$ plates. The successful transformations were verified with an amplicon screening, as seen in figure 3.5 a). The small-scale expression of the native and His-tagged OXA-23 constructs gave a weak induction in the Rosetta2(DE3)plysS and BL21(DE3)plysS cell lines (for His-tagged OXA-23), and a stronger induction in the Arctic Express cell line (figure 3.5, b)). The large-scale expression in the Arctic Express cell line gave no induction of the native or the His-tagged OXA-23 construct. It was also attempted to express the OXA-23 constructs in the *E. coli* cell line BL21(DE3)pRare, but with a negative result with respect to induction of the OXA-23 constructs.

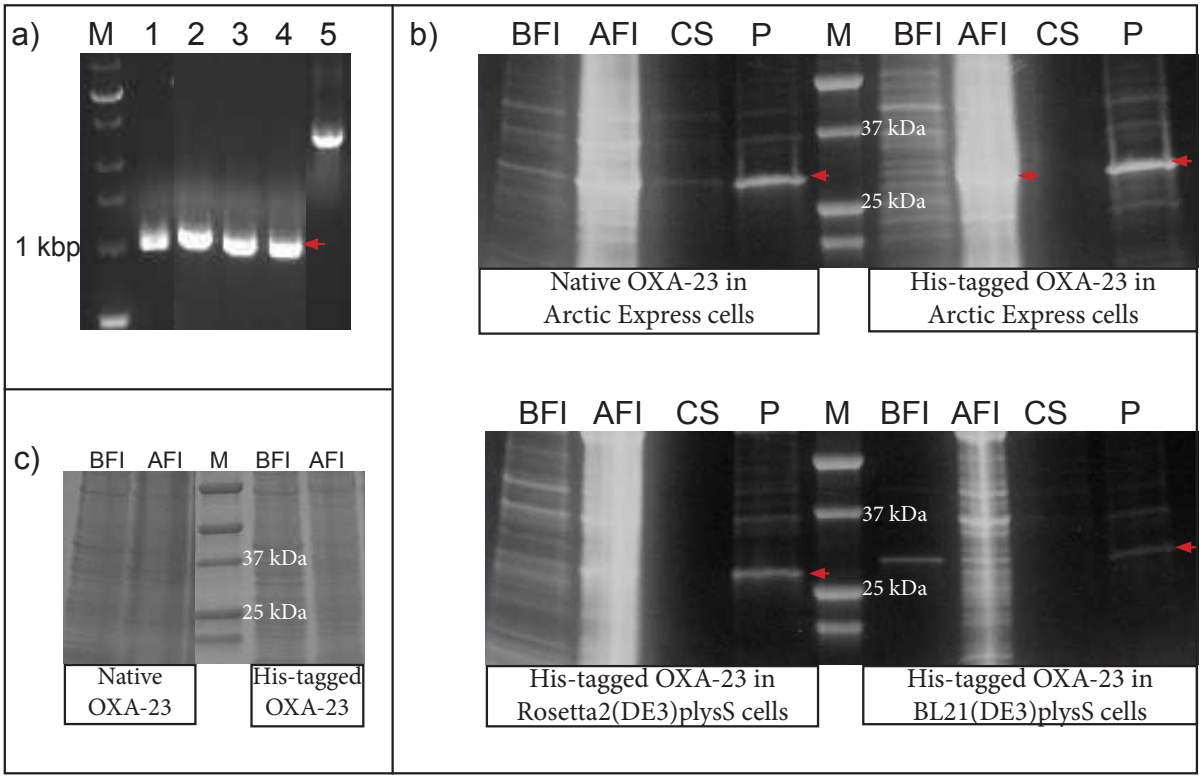

Figure 3.5: The agarose gel results from the amplicon screening (**a**) and the SDS-PAGE results from the small-scale (**b**) and large-scale (**c**) expression of native and His-tagged OXA-23. **a)** The agarose gel results from the amplicon screening. The M lane is the Perfect DNA 1 kbp marker, with the 1 kbp-sized band marked. Lane 1 is the native OXA-23 construct in *E. coli* cell line Arctic Express. Lane 2 is His-tagged OXA-23 in Arctic Express. Lane 3 is His-tagged OXA-23 in Rosetta2(DE3)plysS. Lane 4 is His-tagged OXA-23 in BL21(DE3)pRare. The expected sizes of the constructs from the T7 promoter to the T7 terminator can be found in table 3.5. Lane 5 is the pDEST17 vector used as a positive control. **b)** The SDS-PAGE results from the small-scale expression of native and His-tagged OXA-23 in Arctic Express cell (top figure) and His-tagged OXA-23 in Rosetta2(DE3)plysS and BL21(DE3)pRare cells (bottom figure). The bands of relevant size are indicated with an arrow. The clearest induction can be seen in the P-bands (pellet sample after sonication) in the Arctic Express cells. The Rosetta2(DE3)plysS cells has a weaker induction. The band shown with an arrow in the BL21(DE3)plysS cells is also present in the BFI sample band, indicating that the protein has not been over-expressed after induction. **c)** The SDS-PAGE results from the large-scale expression of native and His-tagged OXA-23 in Arctic Express cells. As can be seen in the AFI bands for both the native and the His-tagged OXA-23 constructs, there are no bands at relevant size to indicate over-expression of the protein.

Protein expression of native OXA-24

It was attempted to express the native OXA-24 construct in a series of different LB and TB volumes using the *E. coli* cell line BL21(DE3)pLysS as expression host, with little consistency in the induction results. An overview of the induction results is presented in table 3.6, with the induction being classified as strong, weak or no induction.

Table 3.6: The results from expression attempts of OXA-24. The OXA-24 protein was induced consistently at smaller volumes (5-50 mL). At larger volumes, which is more convenient for over-expression of protein, the SDS-PAGE analysis showed either very weak, or no induction of the protein. The 400 mL TB expression was found to be weak, but the ion-exchange purification attempt yielded no protein.

Medium	**Volume**	**Induction**	**# of samples**
LB medium	5 mL	Strong	9
		Weak	2
		Non	0
	10 mL	Strong	2
		Weak	0
		Non	0
	50 mL	Strong	2
		Weak	0
		Non	0
	100 mL	Strong	1
		Weak	0
		Non	10
	250 mL	Strong	0
		Weak	1
		Non	0
	500 mL	Strong	0
		Weak	0
		Non	2
TB medium	400 mL	Strong	0
		Weak	(2)
		Non	0
	1000 mL	Strong	0
		Weak	0
		Non	2

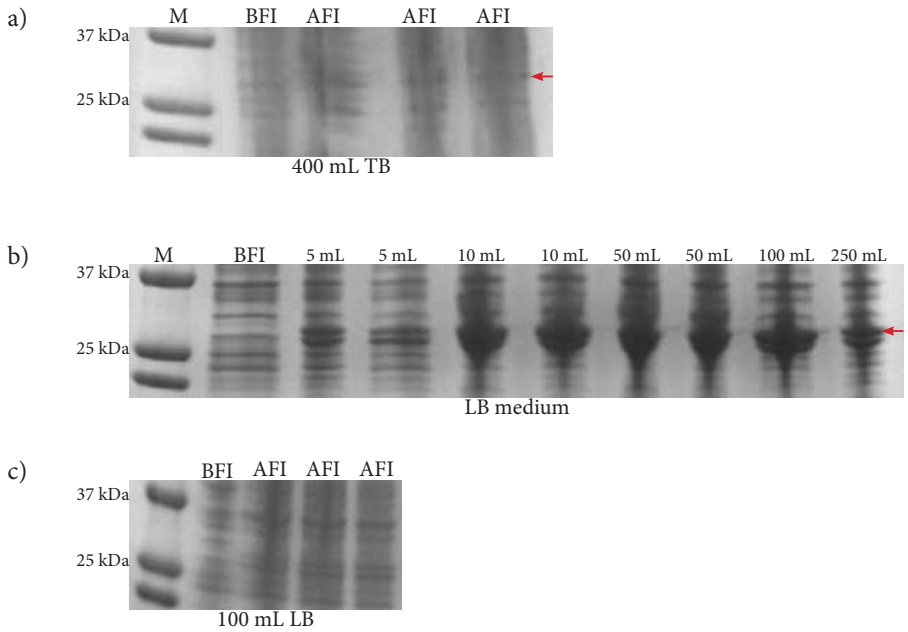

Figure 3.6: SDS-PAGE results from induction attempts of OXA-24 in 400 mL TB medium (a), a series of 5-250 mL LB medium (b), and multiple samples of 100 mL LB medium. **a)** These samples of expression in 400 mL TB showed a very weak induction as indicated by the red arrow. It was attempted to purify these samples, but without any yield. **b)** The SDS-PAGE results from the expression series of LB volumes from 5 mL to 250 mL. The strongest induction was in the 10 mL, 50 mL and 100 mL samples. **c)** The attempt to express OXA-24 in 10 samples of 100 mL LB did not show induction for any of the samples.

3.1.4 Ion-exchange purification of native OXA-24

Figure 3.7 shows the chromatogram from the ion-exchange purification of OXA-24 at column pH 7.2, in Buffer A. The FT samples tested positive on the nitrocefin test, as the sample changed color from yellow to red when a small amount of nitrocefin was added.

Figure 3.8 shows the chromatogram from the second ion-exchange purification where the pH gradient from 9.5-6.5 was run. There was a small shift in the fraction numbers on the chromatogram compared to the fractions being eluted. Fractions 38-43 tested weakly positive towards nitrocefin. The SDS-PAGE analysis (figure 3.9) of fractions 36-46 did not show any bands of appropriate sized protein, but it did show bands at approximately 15 kDa, indicating that the protein sample, if containing the OXA-24 enzyme, is not pure enough to use in enzyme kinetics.

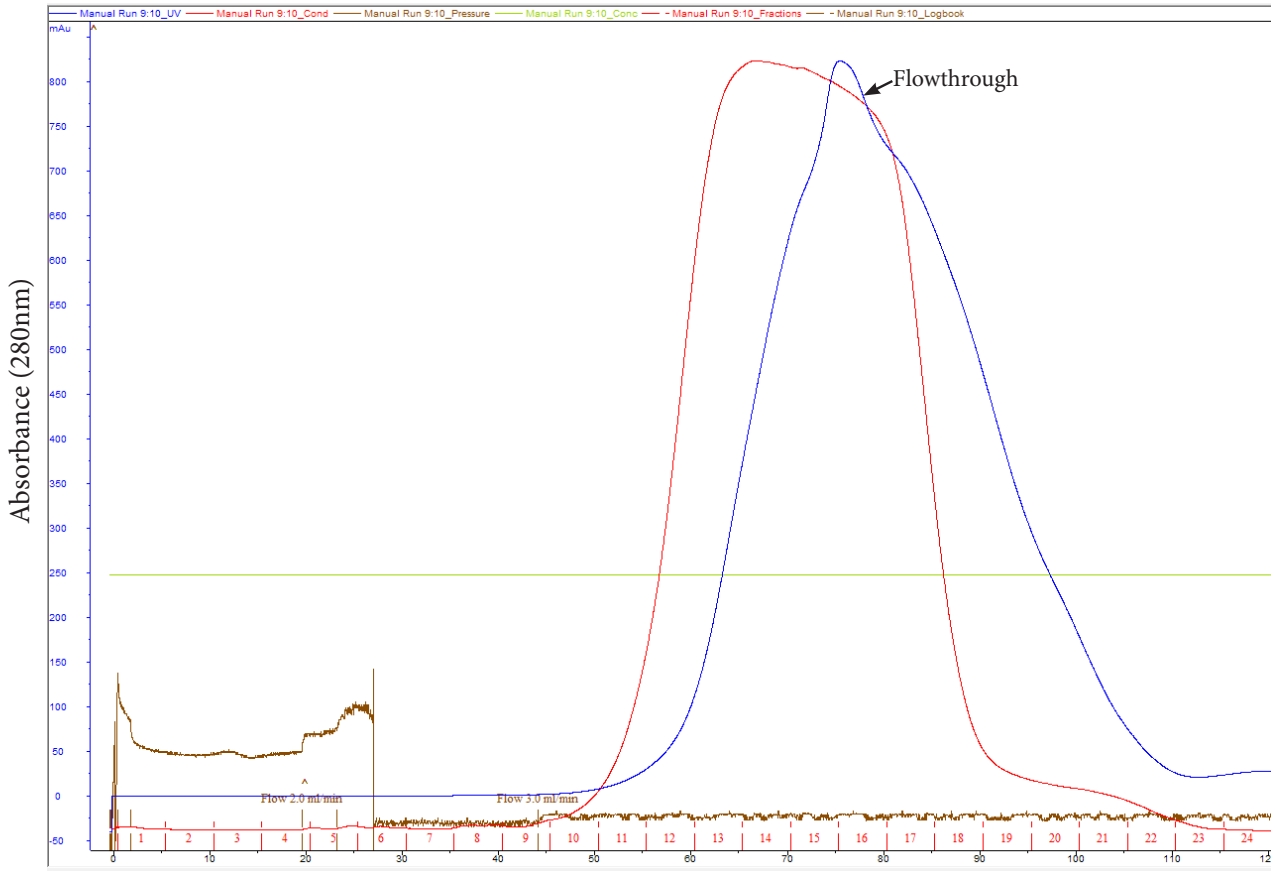

Figure 3.7: The purification chromatogram showing the FT from the anion-exchange purification of the native OXA-24 construct with an approximate OD_{280} (blue line) of 850 mAu. Fractions 12-22 were taken to the next purification step.

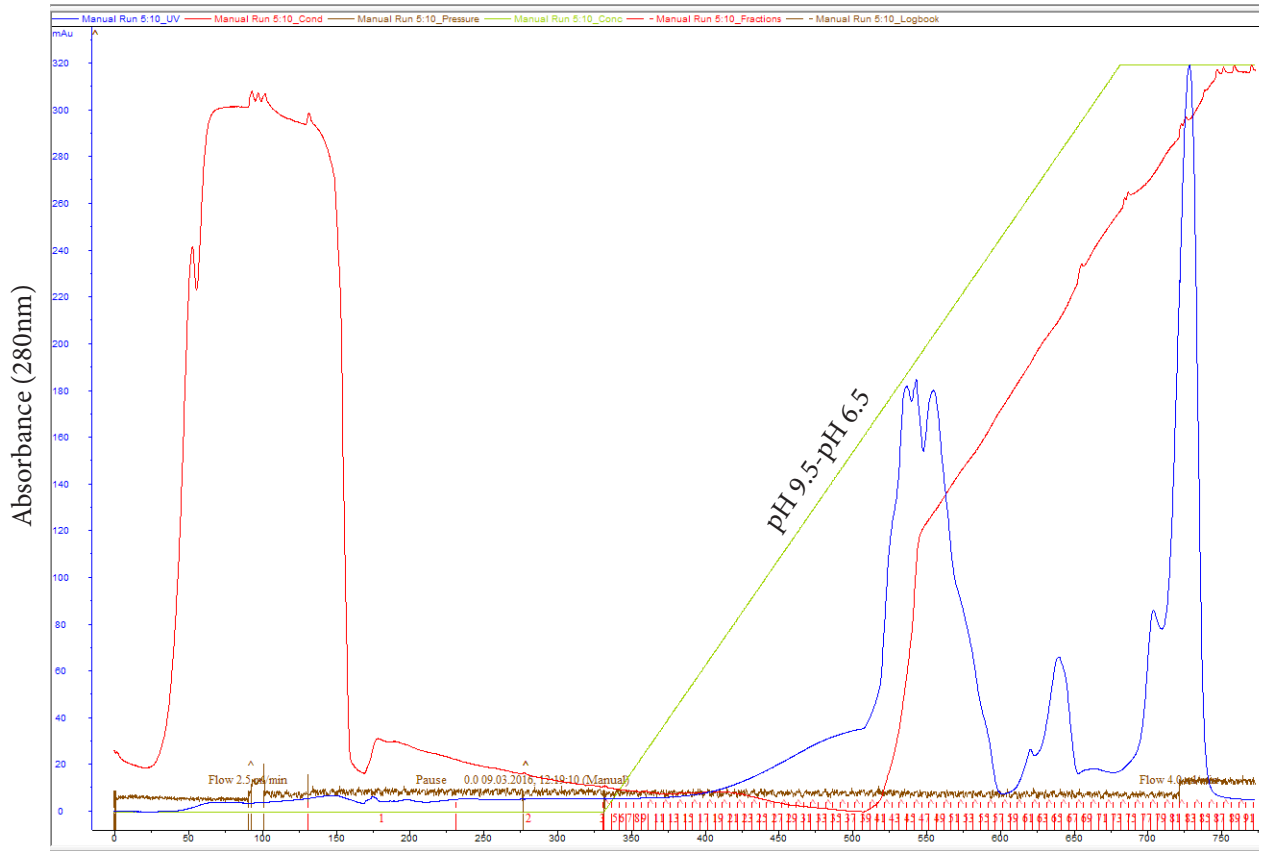

Figure 3.8: The chromatogram from the second anion-exchange purification, where a pH gradient was run from pH 9.5 to pH 6.5. The green line shows the gradient from 0-100% towards pH 6.5.

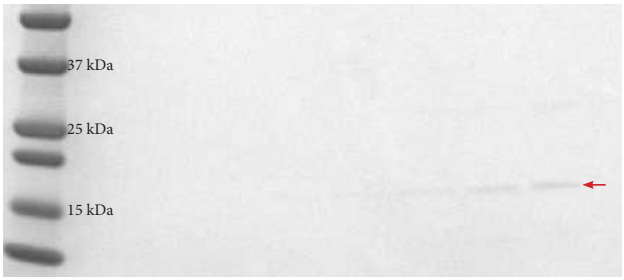

Figure 3.9: The SDS-PAGE analysis of F36-F46 (shown in figure 3.8). The amount of protein was too low to show up on the gel, and given that bands of smaller size did show up, the protein would not have been pure enough to use in enzyme kinetics. The bands indicated with the red arrow is a smaller contaminant more prominent in the gel than the target OXA-24 enzyme.

3.1 OXA-48 mutations S118G, R206A and R250A

3.1.1 Site-directed mutagenesis of OXA-48

Phusion mutagenesis reaction and transformation of bla_{OXA-48} mutants.

The Phusion mutagenesis reaction was carried out to create the three bla_{OXA-48} mutants, followed by a transformation to *E. coli* XL1-blue cells. The amplicon screening suggested a successful transformation, as can be seen in figure 3.10. Lanes 1-3 shows the mutants S118G, R206A and R250A, respectively; lane 4 shows the native pDEST17 construct used as a positive control; all the bands corresponds to the expected sizes of the bla_{OXA-48} mutants and native pDEST17 construct listed in table 3.7.

Table 3.7: The expected sizes of the native pDEST17 construct and the bla_{OXA-48} constructs after the amplicon PCR, which uses a T7 fwd. primer and a T7 rev. primer (table 2.2) to create constructs from the T7 promoter region and the T7 terminator region in the vector. The bla_{OXA-48} gene is inserted in between these regions.

Construct	**Size of gene construct from T7 promoter to T7 terminator (bp)**
Native pDEST17	1896
bla_{OXA-48} mutants	958

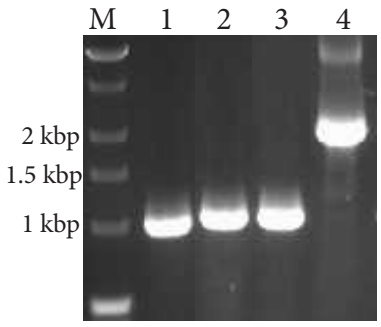

Figure 3.10: The gel electrophoresis results from the amplicon PCR of the bla_{OXA-48} mutants. The M lane is the Perfect DNA marker 0.1-12 kbp with relevant bands marked. Lanes 1, 2 and 3 shows mutants S118G, R206A and R250A, respectively. Lane 4 shows the native pDEST17 vector used as a positive control. All the bands correspond to the expected sizes listed in table 3.7.

Big Dye 3.1 sequencing results of bla_{OXA-48} mutants S118G, R206A and R250A

The three mutated pDEST17 bla_{OXA-48} plasmids were purified following the Wizard *Plus* SV Minipreps DNA Purification System protocol, followed by a concentration measurement at OD_{260nm} to the concentrations listed in table 3.8, which found the DNA concentrations to be 40-56 ng/μL for the three mutants. After Big Dye 3.1 sequencing PCR, the three bla_{OXA-48} mutants were sent to the sequencing laboratory at the University Hospital of North Norway for sequencing. The program SnapGene viewer [60] was used to view the sequencing chromatograms, and the program BLASTN 2.3.1+ [59] was used for sequence alignment with the wild type bla_{OXA-48} sequence (modified to have the signal sequence removed and a His-tag and TEV-cleavage site added) (GenBank: AAP70012) [29] to confirm the mutated sequences. The sequence chromatograms confirming the three OXA-48 mutations are shown in figure 3.11.

The bla_{OXA-48} S118G alignment gave identities = 805/807 (99%) and gaps = 0/807 including the His-tag and TEV-site, the two nonmatching bps corresponds to the target mutation.

The bla_{OXA-48} R206A alignment gave identities = 804/807 (99%) and gaps = 0/807. Two of the nonmatching bps corresponds to the target mutation, and the last can be explained in the chromatogram as a sequencing error.

The bla_{OXA-48} R250A alignment gave identities = 802/807 (99%) and gaps = 1/807. The nonmatching bps that does not correspond to the target mutation, can be explained in the chromatogram as sequencing errors.

The sequencing results indicated successful mutations in all three bla_{OXA-48} constructs, as well as correct overall sequences.

Table 3.8: The DNA concentrations of the three pDEST17 bla_{OXA-48} mutants after plasmid purification, after measuring OD_{260}.

OXA-48 mutant	**DNA concentration (ng/μL)**
S118G	40
R206A	33
R250A	56

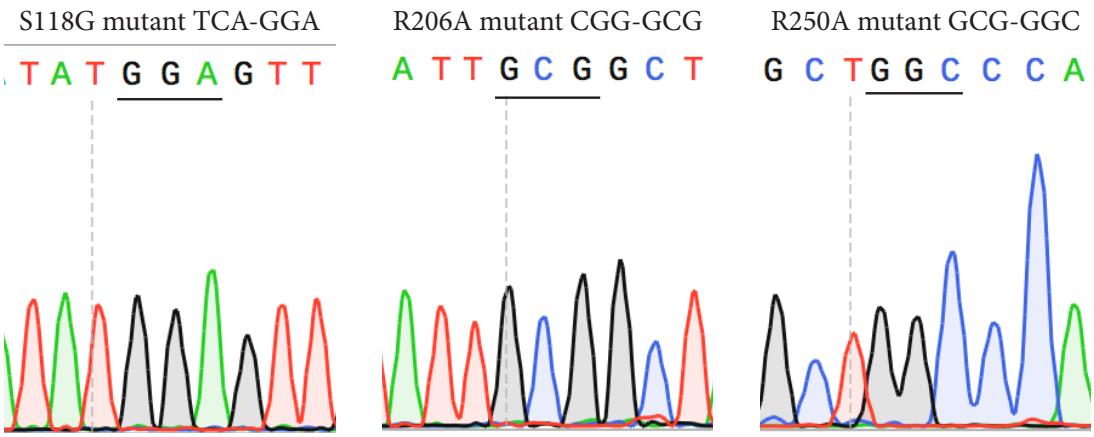

Figure 3.11: The sequencing results showed the mutations for the three OXA-48 constructs S118G (left), R206A (middle) and R250A (right), as underlined in the figure. The R250A mutation is located in the end of the gene, which gives poorer sequencing quality scores [62] as can be seen in the uneven peaks (right figure). But the mutation was showing in both the fwd. and rev. sequencing of the R250A mutant (rev. sequence shown), strongly indicating a successful mutagenesis.

3.1.2 Protein expression of OXA-48 mutants S118G, R206A and R250A

Table 3.9: The sizes of the three OXA-48 mutants, before and after TEV-cleavage of His-tag. This is done in between two HisTrap purification steps. All sizes are without the signal sequence.

OXA-48 mutant	**Molecular weight (kDa), before TEV cleavage**	**Molecular weight (kDa), After TEV cleavage**
S118G	31.187	28.173
R206A	31.132	28.118
R250A	31.132	28.118

Small and large scale protein expression of OXA-48 mutants in expression host BL21Star(DE3)pRare

In figure 3.12, a), which shows the gel electrophoresis results from the amplicon screening after transformation the the *E. coli* cell line BL21Star(DE3)pRare, lanes 1-3 shows the S118G mutant, lanes 4-6 shows the R206A mutant and lanes 7-9 shows the R250A mutant. The M lane is the Perfect DNA marker 0.1-12 kbp with relevant bands marked, and lane 10 is the native pDEST17 vector used as positive control. The three OXA-48 mutants were successfully transformed into the *E. coli* cell line BL21Star(DE3)pRare as can be seen in figure 3.12 a), where all the bands corresponds with the expected sizes listed in table 3.9.

The *E. coli* cell line BL21Star(DE3)pRare had been used successfully as expression host for wild type OXA-48 by Ph.D. student Bjarte A. Lund [39], so this was the only cell line used in the protein expression of the OXA-48 mutants. As can be seen in figure 3.12 b) and c), the small and large scale protein expression resulted in induction for all three OXA-48 mutants.

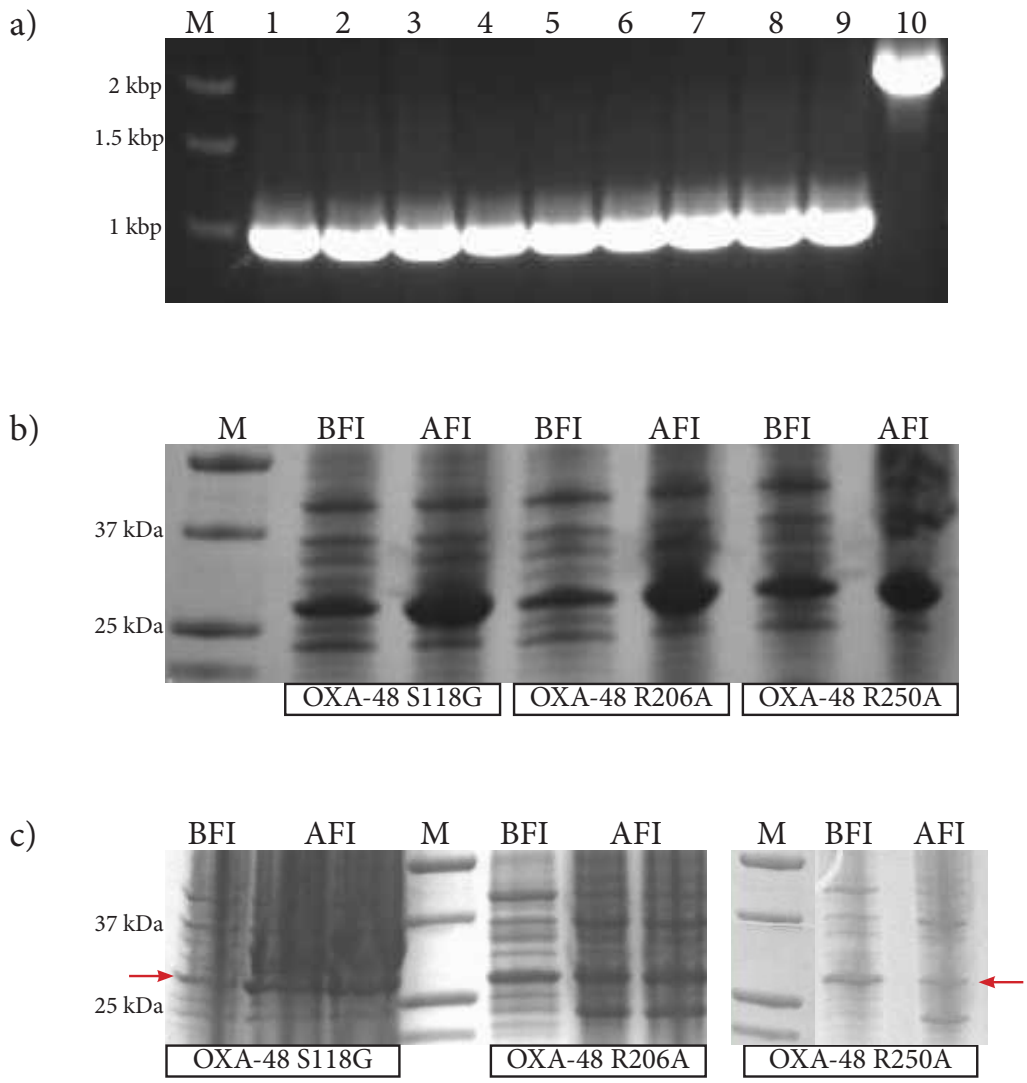

Figure 3.12: The gel electrophoresis results from the amplicon screening after transformation to *E. coli* cell line BL21Star(DE3)pRare, and SDS-PAGE results from the small and large scale protein expression of OXA-48 mutants S118G, R206A and R250A. **a)** The amplicon screening results showed DNA bands corresponding to the expected sizes of the three OXA-48 mutants after amplicon PCR, indicating a successful transformation. Lanes 1-9 are the three OXA-48 mutants with three samples for each mutant. Lane 10 is the native pDEST17 vector. **b)** The SDS-PAGE analysis from the small scale protein expression showed induction for all three OXA-48 mutants. **c)** The SDS-PAGE analysis from the large scale protein expression in 1 L TB also showed induction for all three OXA-48 mutants, as can be seen in the bands in between the two red arrows. The induction is slightly weaker than the small scale expression, but still considered strong enough for harvesting and purification.

3.1.3 Immobilized metal ion affinity chromatography (IMAC) purification of OXA-48 mutants S118G, R206A and R250A

Affinity purification of OXA-48 mutant S118G, HisTrap step 1

The first HisTrap step, where the His-tagged OXA-48 S118G mutant binds the column and is eluted by a gradient of imidazole-containing Buffer E, separated the target enzyme from a great amount of contaminants, as can be seen in figure 3.13, a). The FT peak has an absorbance of around 3300 mAu, and the OXA-48 S118G peak has an absorbance of around 2200 mAu. The SDS-PAGE analysis (figure 3.13, b)) showed some impurities, but a good protein yield. Fractions 29-38 were pooled and purified in a second affinity purification step.

Affinity purification of OXA-48 mutant S118G, HisTrap step 2

The second HisTrap step, where the His-tag have been cleaved off by TEV protease so that the OXA-48 S118G mutant is eluted in the FT, gave a highly pure protein with a good yield. The OXA-48 S118G peak in the purification chromatogram (figure 3.14, a)) has an absorbance of around 1800 mAu. The SDS-PAGE analysis (figure 3.14, b)) showed a good protein yield and purity of >95%.

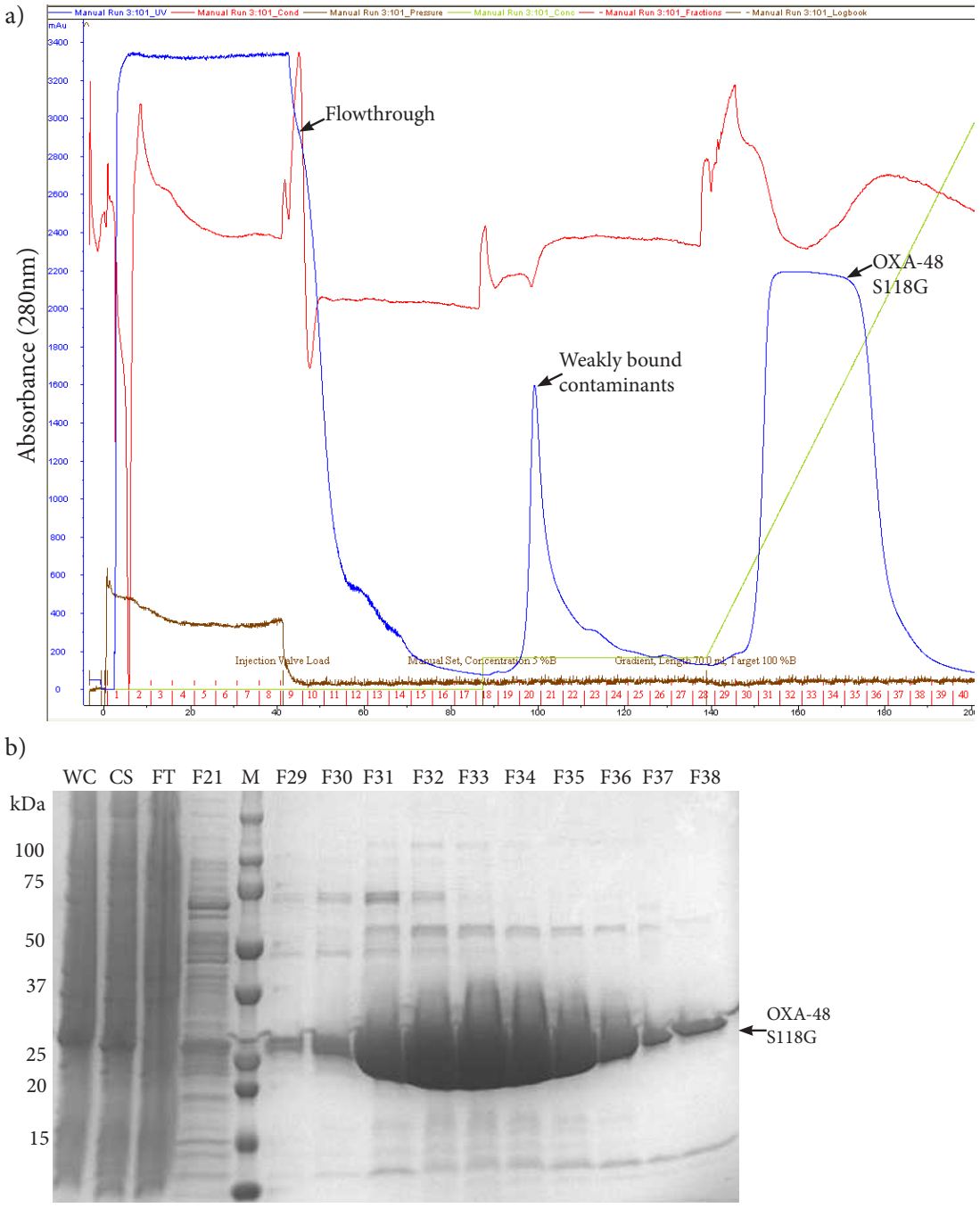

Figure 3.13: Affinity purification and SDS-PAGE analysis of OXA-48 S118G. **a)** The purification chromatogram shows that the first HisTrap step succeeded in separating the target protein from a great amount of contaminants. **b)** The M lanes is the Precision plus protein markers (Bio-Rad) with relevant sizes written to the left. The WC, CS and FT lanes are the whole cell sample, the cell supernatant sample and the FT sample. The SDS-PAGE analysis showed a good protein yield after the first HisTrap step, but the sample still have some impurities. Fractions F29-F38 were pooled and purified in a second step.

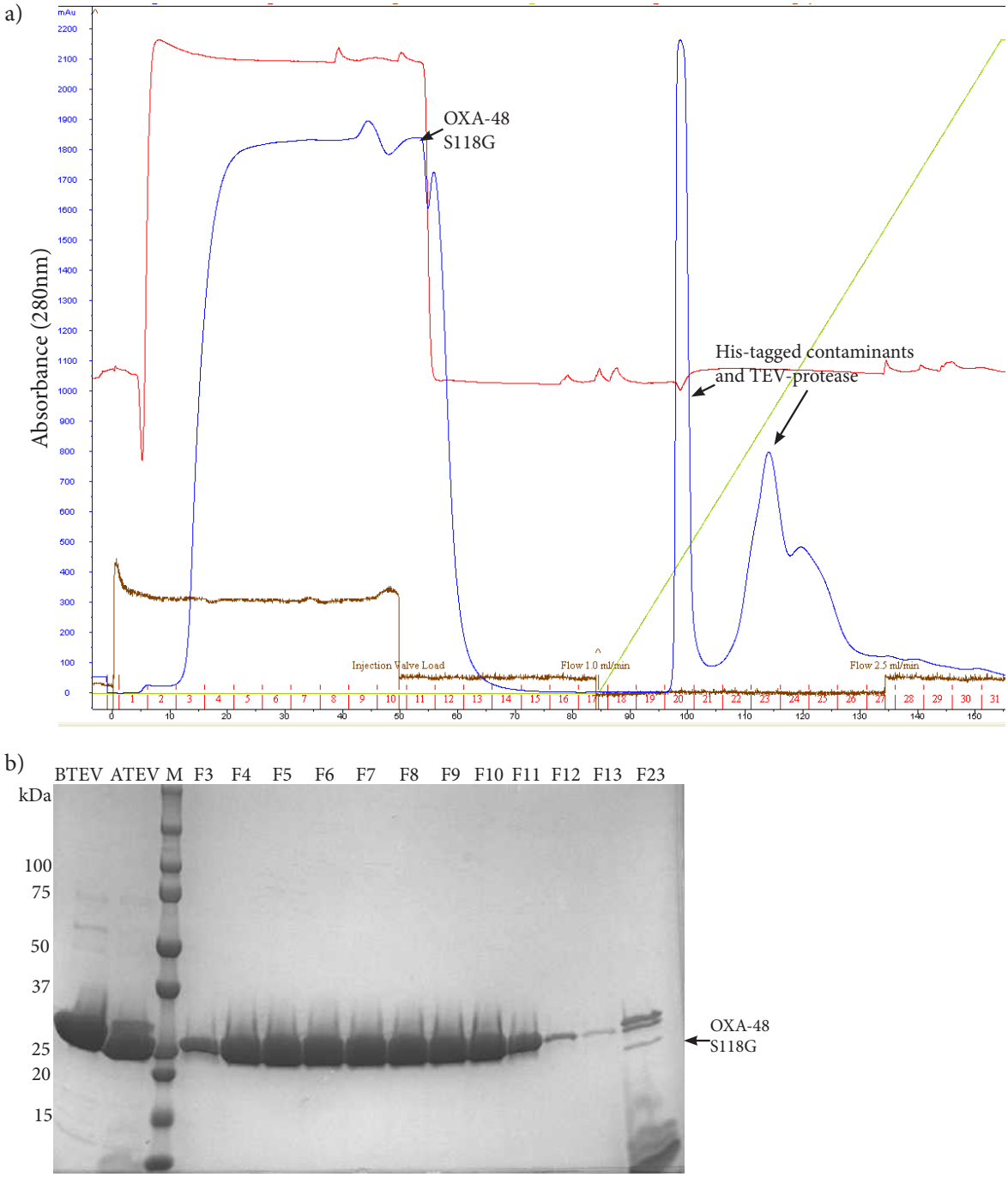

Figure 3.14: Affinity purification and SDS-PAGE analysis after cleavage of His-tag. **a)** The OXA-48 S118G peak in the purification chromatogram has an absorbance of around 1800 mAu, which indicates a very good protein yield. The contaminant peaks show that the second purification step succeeded in separating the target protein from contaminants. **b)** The BTEV and ATEV lanes are samples from before and after TEV-cleavage of the His-tag. The ATEV band is slightly smaller in size than the BTEV band, indicating a successful cleavage as the His-tag region at the end of the protein is no longer there. Lanes F3-F13 is the FT, containing the target OXA-48 S118G mutant; the gel indicates a pure protein with good yield. The F23 lane is a sample from the contaminant peak.

Affinity purification of OXA-48 mutant R206A

The purification chromatograms from the affinity purification of OXA-48 R206A are not shown, as they have a similar structure to the chromatograms from the purification of OXA-48 S118G, and the SDS-PAGE analysis figures gives the most accurate results with respect to purity and yield. The SDS-PAGE analysis shows that the first HisTrap purification step (figure 3.15, a) succeeded in separating the target OXA-48 R206A enzyme from most contaminants, and gave a good protein yield. In figure 3.15 a, F29-F37 are the fractions from the elution of the target protein; since bands corresponding to the size of OXA-48 R206A is most prominent in F32-F37, these fractions were pooled and further purified.

The SDS-PAGE analysis after the second HisTrap purification step indicated that the target OXA-48 R206A enzyme was >95% pure with a good protein yield. This can be seen in figure 3.15, b) F3-F9, where the only bands visible on the gel corresponds to the size of the OXA-48 R206A enzyme.

Affinity and ion-exchange purification of OXA-48 mutant R250A

From the first HisTrap purification step of OXA-48 R250A (figure 3.16, a) one can see that the enzyme is prominent in the elution fraction (F42-F50), but with many impurities. Based on this figure, fractions 44-50 were collected and pooled for further purification. The second HisTrap purification step (figure 3.16, b) yielded a good amount of protein (F2-F12) but the samples still have a lot of impurities (marked with red arrows in the figure). Based on this, the F2-F12 samples were collected and pooled for a third purification step using an anion exchange column. The chromatogram and SDS-PAGE analysis from this purification step is shown in figure 3.17 and 3.18, respectively. The F2-F11 lanes are the fractions from the FT containing the OXA-48 R250A enzyme; they show a successful purification with a good protein yield and >95% purity.

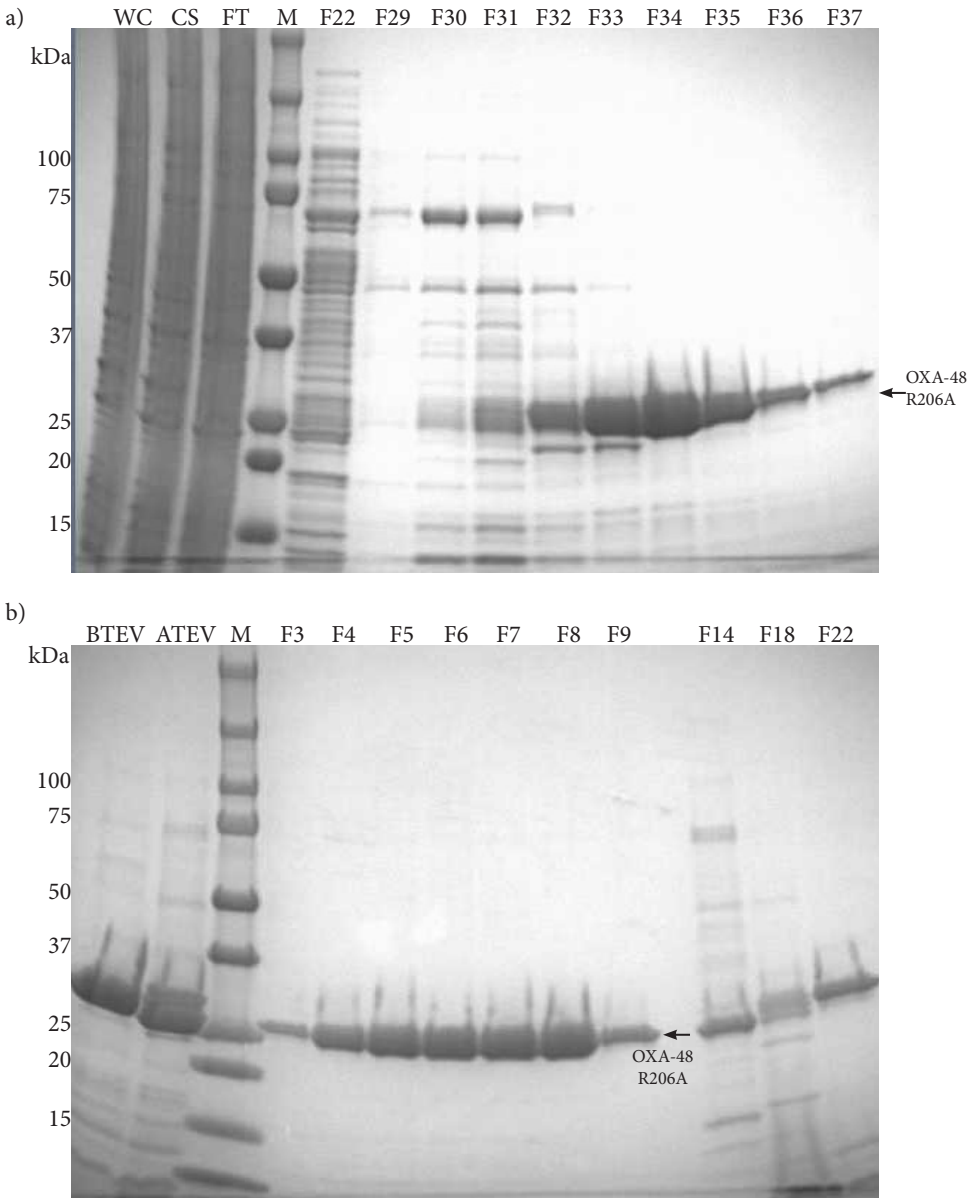

Figure 3.15: SDS-PAGE analysis from HisTrap purification step 1 (a) and HisTrap purification step 2 (b) of OXA-48 R206A. **a)** SDS-PAGE analysis from the first HisTrap purification step, where the His-tagged OXA-48 R206A enzyme binds to the column before being eluted with Imidazole containing Buffer E. The F22 lane is a sample from the second contaminant peak where weakly bound contaminants are eluted with 5% Buffer E. F29-F37 are the fractions from the Buffer E gradient elution. Based on this figure, fractions 32-37 were collected and pooled for further purification, as these fractions seem to contain a good amount of target protein. F30 and F31 also contains the target OXA-48 R206A mutant, but they seem to contain more contaminants than they do target protein. **b)** SDS-PAGE analysis from the second HisTrap purification step, where the His-tag has been cleaved off the target OXA-48 R206A enzyme. The band in the ATEV lane is slightly smaller than the BTEV band, indicating a successful cleavage. F3 to F9 is samples from the FT, where the target OXA-48 R206A enzyme is eluted. The enzyme seems to be >95% pure with a good yield. F14, F18 and F22 are contaminant peaks.

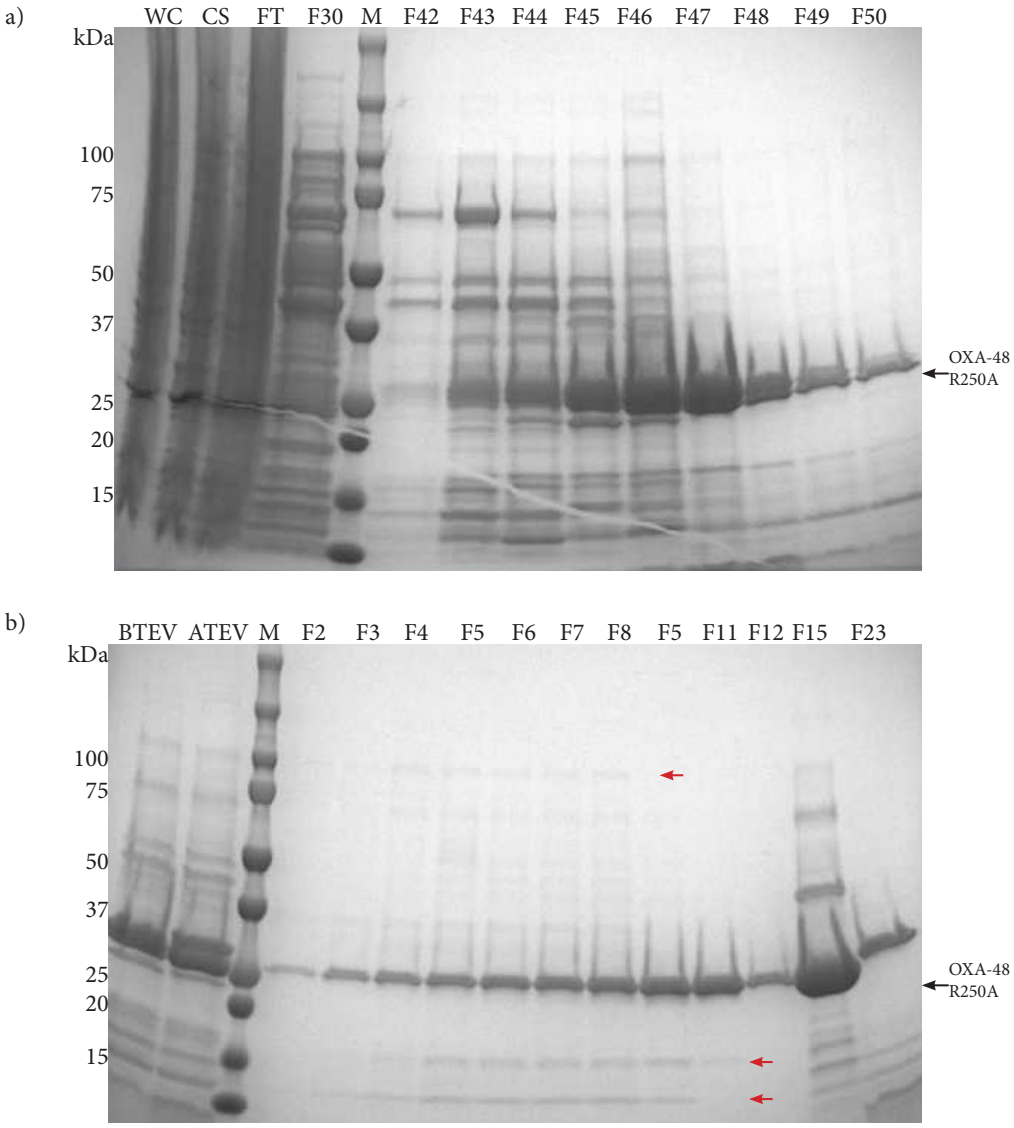

Figure 3.16: The SDS-PAGE analysis results from the HisTrap purification step 1 (a) and HisTrap purification step 2 (b). **a)** F42-F50 are the fractions form the Buffer E gradient elution. The samples contain a good amount of the target protein, but also a good amount of contaminants. Based on this figure, F44-F50 were collected and pooled for further purification. F30 is the contaminant peak from the 5% Buffer E wash. **b)** F2-F12 are the fractions from the FT, containing the OXA-48 R250A enzyme. The samples seem to still contain contaminants, as marked with red arrows in the figure. The samples F2-F12 were therefore pooled and further purified in an anion exchange purification. F15 and F23 are samples from the contaminant peaks from the Buffer E elution. The strong band in F15 has the same size as the target protein bands, but should contain mostly the TEV-protease enzyme which has a size of 27 kDa.

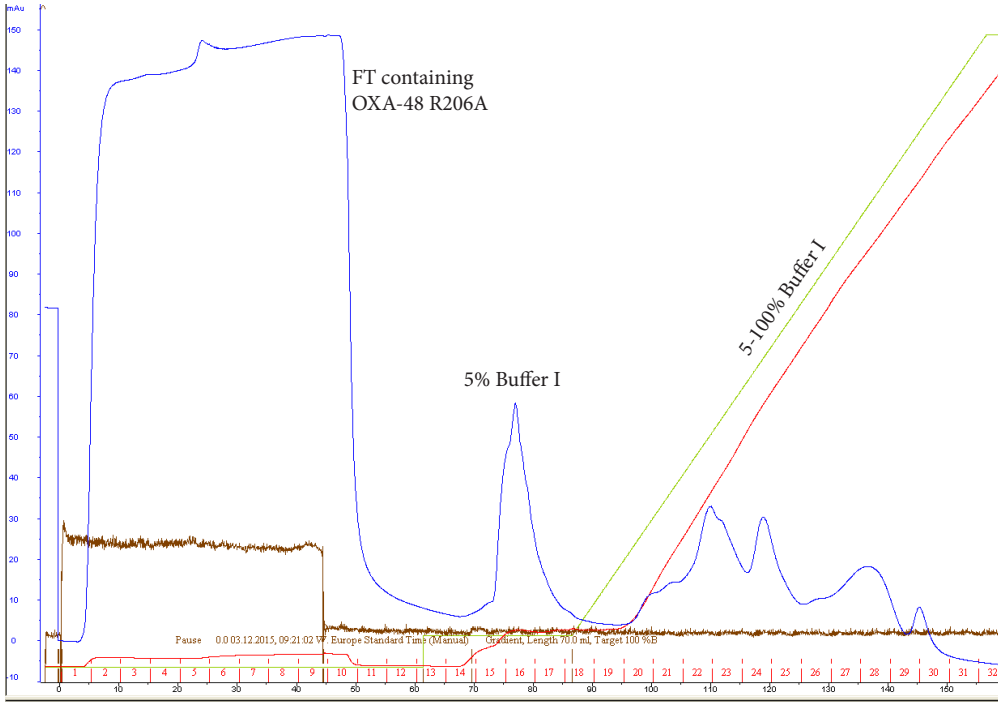

Figure 3.17: Anion exchange chromatogram from the purification of OXA-48 R250A mutant. The mutant was eluted in the FT, the peak has an absorbance of around 150 mAu.

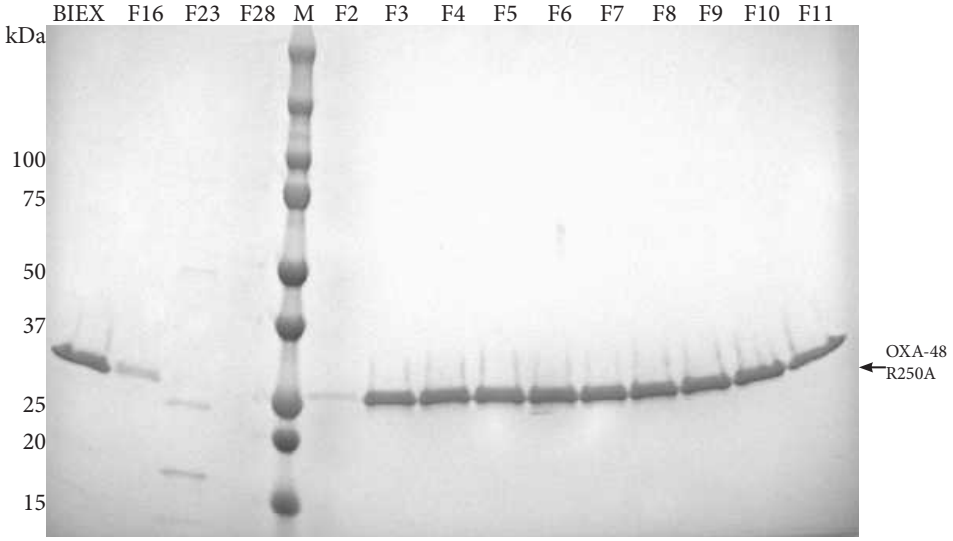

Figure 3.18: SDS-PAGE analysis from the anion exchange purification of OXA-48 R250A. Since the target enzyme is positively charged at pH 7.2, which is the pH of the buffer used in the anion exchange column, the OXA-48 R250A enzyme is eluted in the FT. The BIEX lane is a sample from before running the ion-exchange purification. F2-F11 are the FT fractions containing the target enzyme. From these fractions one can see that the OXA-48 R250A enzyme is >95% pure, and the yield is good. F16, F23 and F28 are contaminant peaks.

Concentration of OXA-48 mutants S118G, R206A and R250A

The OXA-48 S118G mutant was concentrated to 13.9 mg/mL with a total protein amount of 173 mg. The OXA-48 R206A mutant was concentrated to 16.7 mg/mL with a total protein amount of 50 mg. The OXA-48 R250A mutant was concentrated to 8 mg/mL with a total protein amount of 12 mg.

3.1.4 Protein crystallization, X-ray data collection and modelling of the three OXA-mutants S118G, R206A and R250A

Crystallization of OXA-48 mutants S118G, R206A and R250A

The initial crystallization trials with the OXA-48 S118G mutant in the three screens KCSG, StockPEG 17 and Tromsostock 41 gave small crystals in several of the conditions. Based on the best looking crystals, the conditions showed in table 2.9 were used for optimization and crystallization of all three OXA-48 mutants. The crystallization screens resulted in several high quality crystals for all three mutants, as can be seen in figure 3.19. The conditions in rows C and D (14-18% PEG MME5K and 0.1 M BisTrisPropane pH 9.0 (row C)/pH 9.5 (row D)) seemed to yield the crystals of highest quality compared to the conditions in row A and row B (38-42% PEG 400 and 0.1 M BisTrisPropane pH 9.0 (row A)/pH 9.5 (row B)).

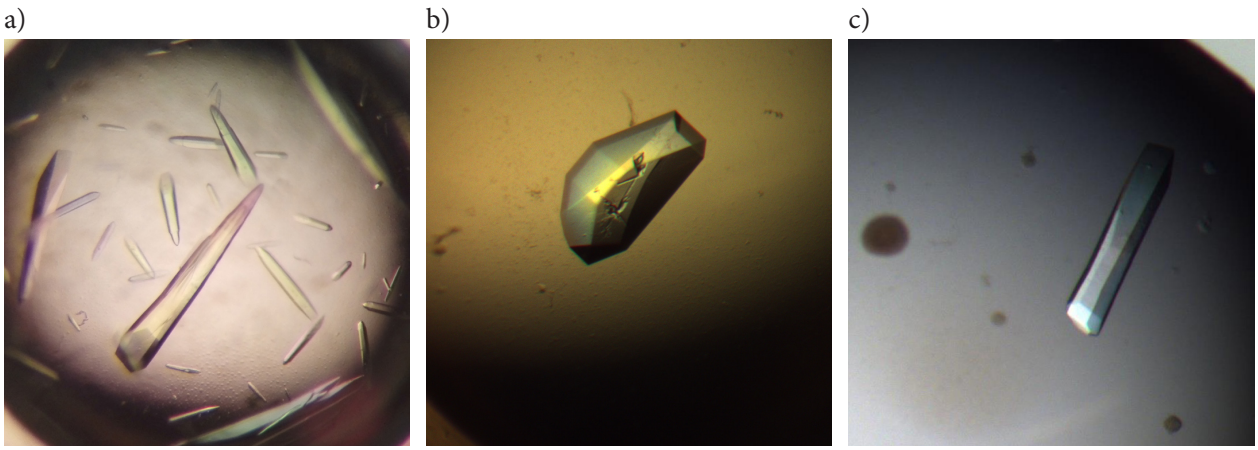

Figure 3.19: Crystals of OXA-48 mutants S118G (a), R206A (b) and R250A (c). All these crystals were obtained in the crystallization condition row C or D, which contained 14-18% PEG MME5K and 0.1 M BisTrisPropane pH 9.0 (row C)/pH 9.5 (row D).

X-ray data collection and structure determination of the three OXA-48 mutants S118G, R206A and R250A

The structures of the three OXA-48 mutants S118G, R206A and R250A were solved to a final resolution of 1.6, 2.6 and 2.4 Ångstrom (Å) using OXA-48 wild type as a search model in molecular replacement (PDB ID: 5DTK) [54]. The structures were obtained with good *R*-factors (0.19-0.16) and R_{free} values (0.28-0.18), as well as favorable geometries. The *R*-factor measures the agreement between the observed reflection intensities (from the experimental dataset) agrees with the corresponding structure factors calculated from the current model [52]. The *R*-factor decreases throughout the refinement, and for a protein model an *R*-factor below 0.2 is considered good. R_{free} is calculated from a set of randomly chosen intensities, in this case 5% of the reflections used in the refinement, that are not used during the refinement. This value is used as a quality control over the refinement process, by measuring how well the calculated model predicts experimental intensities not used during the refinement [63]. The RMSD values are root-mean-square deviations of the model's bond lengths and angles from an accepted set of values, and should not exceed 0.02 for bond lengths and 4° for bond angles [52]. The *B*-factors assess uncertainty in the atom positions in the model, and the Ramachandra diagram plot the ϕ and ψ angles of the backbone of the protein within favored, allowed and outliers regions.

Table 3.10: Data collection and refinement statistics for OXA-48 mutant S118G, R206A and R250A. The numbers in parenthesis are for the highest resolution shell.

Parameter	**S118G**	**R206A**	**R250A**
X-ray source	ID23-2	14.1	14.1
Data collection statistics			
Space group	C 2 2 2_1	P 6_5 2 2	P 6_5 2 2
Unit cell dimensions			
a, b, c (Å)	122.84, 212.82, 162.06	120.15, 120.15, 160.11	122.24, 122.24, 161.02
α, β, λ (°)	90, 90, 90	90, 90, 120	90, 90, 120
Resolution range (Å)	48.95-1.58 (1.64-1.58)	47.49-2.61 (2.7-2.61)	47.87-2.35 (2.43-2.35)
Total reflections	1359139 (126159)	295216 (27309)	414326 (38262)
Unique reflections	287177 (28517)	21396 (2038)	30205 (2885)
Multiplicity	4.7 (4.4)	13.8 (13.4)	13.7 (13.3)
Completeness	1.0 (1.0)	0.99 (0.98)	1.0 (0.98)
Mean ($\langle I \rangle / \langle \sigma I \rangle$)	9.96 (1.20)	10.52 (1.53)	11.07 (1.70)
Wilson B factor (Å^2)	17.96	43.95	32.12
R_{merge} (%)	0.099 (1.121)	0.319 (2.032)	0.299 (1.528)
Refinement statistics			
Reflections used in refinement	287144 (28508)	21374 (2031)	30196 (2884)
Reflections used for R_{free}	14516 (1387)	1069 (101)	1510 (145)
R-factor[a]	0.164 (0.294)	0.194 (0.293)	0.184 (0.243)
R_{free}[a]	0.178 (0.301)	0.282 (0.402)	0.233 (0.334)
Number of non-hydrogen atoms	13745	4045	4296
Macromolecules	11825	4015	4048
Ligands[b]	3	None	9
Protein residues	1447	482	486
RMSD bond lengths (Å)	0.008	0.018	0.016
RMSD bond angles (°)	0.89	1.13	1.06
Ramachandran favored (%)	98	95	98
Ramachandran allowed (%)	2.2	4.3	2
Ramachandran outliers (%)	0	0.61	0
Rotamer outliers (%)	0	1.4	0.47
Clashscore	4.97	5.15	3.54
Avarage B-factor (Å^2)	24.19	47.66	27.48
Macromolecules	22.23	47.74	27.46
Ligands	19.17	None	33.92
Solvent	36.28	37.69	27.62

[a] *R*-factor/$R_{free} = \Sigma h||F_{obs}|-|F_{calc}||/(\Sigma h|F_{obs}|)$, where $|F_{obs}|$ and $|F_{calc}|$ are the observed and calculated structure factor amplitudes for all reflections (*R*-factor) and the reflections used in the R_{free} set.

[b] for the S118G structure, all three ligands are chlorine ions. For the R250A structure there are 8 ethylene glycol molecules (from cryo) and one chlorine ion.

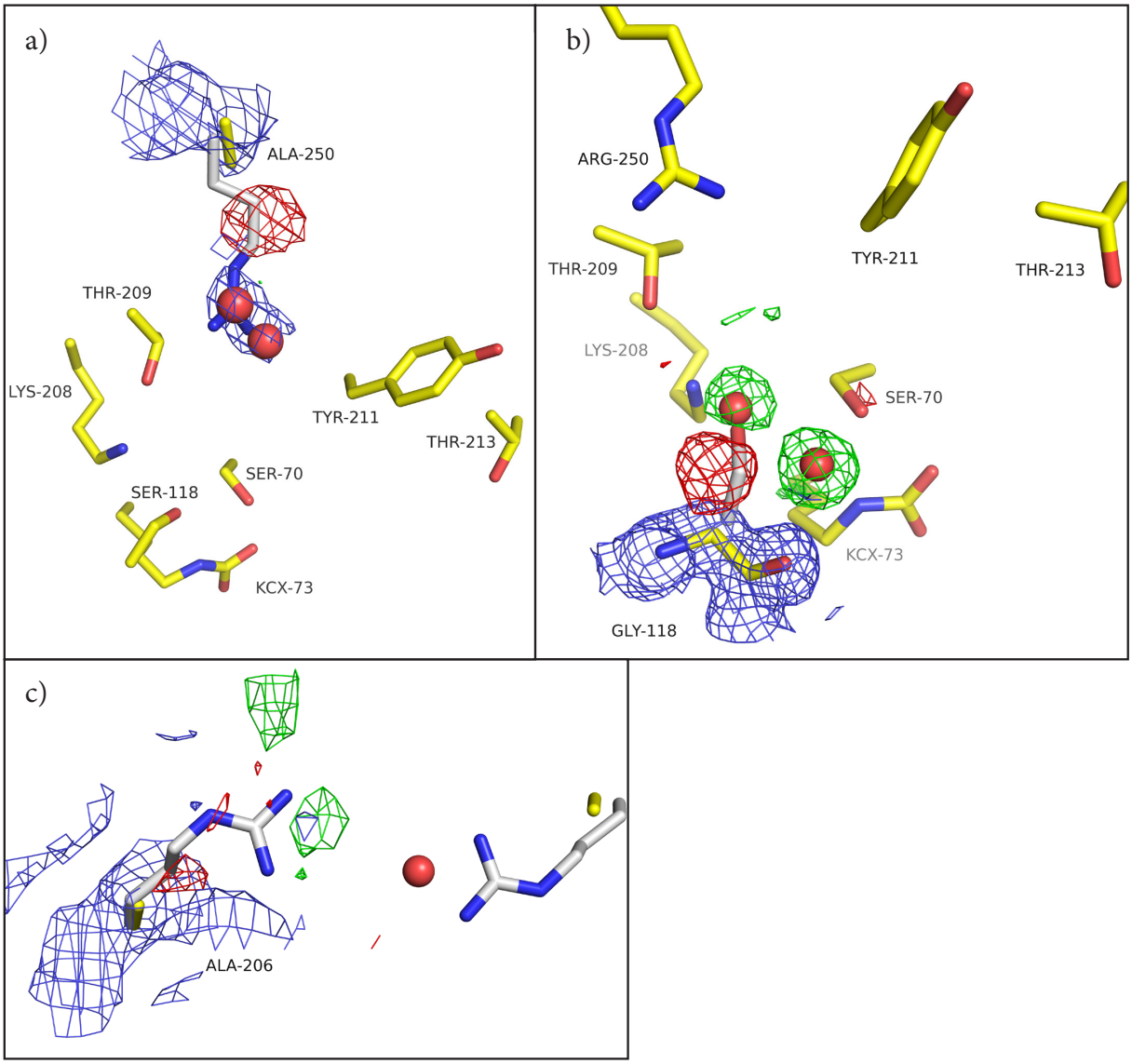

Figure 3.20: Structure maps showing the three mutations R250A (a), S118G (b) and R206A (c). The wild type OXA-48 structure (PDB ID: 3HBR) is superimposed on the mutation structures to illustrate the residues before and after mutation. The residues from the wild type are shown in white sticks, and the residues from the mutation structures are shown in yellow sticks. The electron density maps F_o-F_c (from before mutations were introduced in the structure) and $2F_o$-F_c (after mutations were introduced) are shown to give evidence for the mutations, and the addition of certain water molecules (represented by red spheres). The F_o-F_c maps are displayed at +3.0 σ (green) and -3.0 σ (red) and the $2F_o$-F_c maps are displayed at 1.0 σ (blue) for all structures. **a)** The R250A mutation. The mutation is clearly showing in the map, and the arginine residue has been replaced by two water molecules. **b)** The S118G mutation. Given that the residue is a glycine and lacks a side-chain, the backbone of the structure is shown to illustrate the glycine substitution. The serine residue is absent in the structure, but two water molecules have been inserted. **c)** The R206A mutation. The electron density maps show that the mutation was successful. The chlorine ion bound in the wild type structure seem to be absent in the mutated structure.

The OXA-48 R250A structure

The red electron density in the F_o-F_c map shows an excess of electron density in the model around the wild type arginine residue, which shows a successful mutation to alanine. One can also see that the arginine residue has been replaced by two water molecules.

The OXA-48 S118G structure

Again, the red electron density around the wild type serine residue shown that it is absent, and has been mutated to a glycine residue. The green spheres from the F_o-F_c map represent electron density in the data that is not present in the model, and two water molecules have been inserted here in the refinement. Although the OXA-48 S118G mutant crystal was soaked in avibactam, the inhibitor was not present in the structure map. Comparing the electron density maps from the three mutants, one can clearly see that the S118G mutant was refined to a higher resolution.

The OXA-48 R206A structure

The mutation is evident in the electron density map from the lack of density around the wild type arginine residue. The chlorine ion seems to be absent in the mutated structure, but a water molecule has been inserted in between the mutations. In addition, there seem to be two additional water molecules in the structure, from the green electron density in the F_o-F_c map. Another round of refinement should have been run to add these water molecules.

3.1.5 Enzyme kinetics studies on the three OXA-48 mutants S118G, R206A and R250A

Enzyme kinetics studies were performed with WT OXA-48 and the three OXA-48 mutants S118G, R206A and R250A with the substrates ampicillin (penicillin), nitrocefin, imipenem (carbapenem) and cefepime (cephalosporin). The WT OXA-48 used was a sample previously cloned and purified by Bjarte Lund and Trine Carlsen. The enzyme kinetics results are shown in figure 3.21, and the K_m, k_{cat} and k_{cat}/K_m values are listed in table 3.11, in addition to a comparison of the mutant k_{cat}/K_m values with the WT k_{cat}/K_m values. All the mutants, as well as the WT OXA-48 showed very low activity towards the cephalosporin cefepime, and hence the K_m, k_{cat} and k_{cat}/K_m values are not listed for this substrate. The WT OXA-48 and the OXA-48 mutants also showed lower activity towards the carbapenem imipenem then they did towards ampicillin and nitrocefin.

The OXA-48 R206A mutant have very similar enzyme activity as the OXA-48 WT, when comparing the K_m, k_{cat} and k_{cat}/K_m values in table 3.11, indicating that the mutation did not have an effect on the activity of the enzyme. The OXA-48 S118G and R250A mutants have very low activities when compared to the WT OXA-48, indicating that these mutations in the active site has a negative impact on the activity of the OXA-48 enzyme.

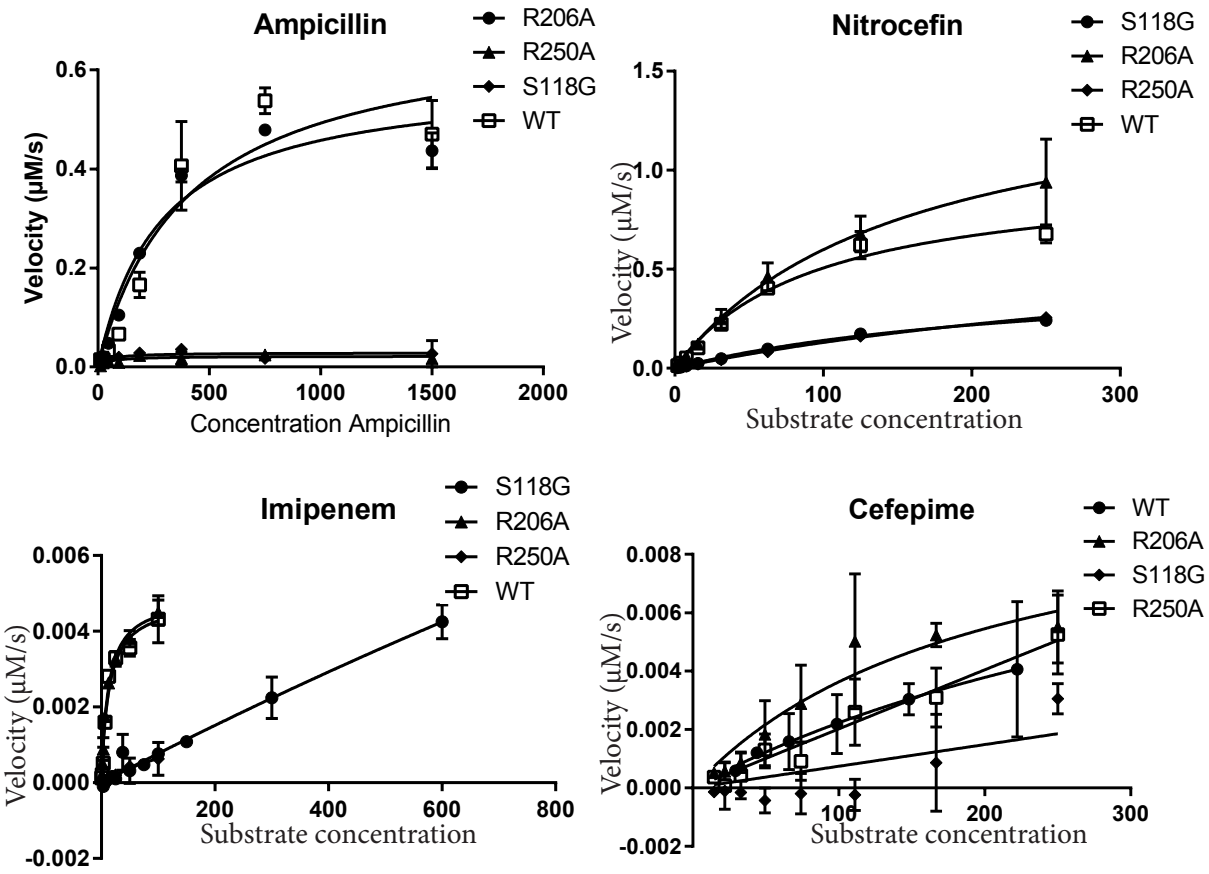

Figure 3.21: Enzyme kinetics results for OXA-48 wild type and OXA-48 mutants S118G, R206A and R250A, where reaction rate is plotted against substrate concentration. The curves for ampicillin, nitrocefin and imipenem show that the OXA-48 WT and the OXA-48 R206A mutant generally have much better catalytic efficiency than the OXA-48 S118G and R250A mutants. The substrate cefepime was not hydrolyzed by any of the enzymes. The OXA-48 WT and R206A mutant also showed lower activity towards imipenem then they did towards ampicillin and nitrocefin.

Table 3.11: K_m, k_{cat} and k_{cat}/K_m values for WT OXA-48 and OXA-48 mutants S118G, R206A and R250A with substrates ampicillin, nitrocefin and imipenem. The enzymes activity towards cefepime was too poor to give values.

Substrate	**OXA-48 S118G**			
	K_m (μM)	**k_{cat} (s^{-1})**	**k_{cat}/K_m ($M^{-1}s^{-1}$)**	$\frac{(k_{cat}/K_m)mutant}{(k_{cat}/K_m)WT}$
Ampicillin	41.2	28.5	691 x 10^3	0.4
Nitrocefin	251.5	493	1960 x 10^3	0.2
Imipenem	5541	43.46	7.8 x 10^3	0.02
	OXA-48 R206A			
Substrate	**K_m (μM)**	**k_{cat} (s^{-1})**	**k_{cat}/K_m ($M^{-1}s^{-1}$)**	
Ampicillin	281.4	586.4	2083 x 10^3	1.2
Nitrocefin	154.5	1523	9857 x 10^3	0.95
Imipenem	12.1	4.9	404 x 10^3	1.1
	OXA-48 R250A			
Substrate	**K_m (μM)**	**k_{cat} (s^{-1})**	**k_{cat}/K_m ($M^{-1}s^{-1}$)**	
Ampicillin	47.1	21.8	462 x 10^3	0.3
Nitrocefin	471.9	743.9	1576 x 10^3	0.15
Imipenem	200.5	1.9	9.48 x 10^3	0.02
	OXA-48 WT			
Substrate	**K_m (μM)**	**k_{cat} (s^{-1})**	**k_{cat}/K_m ($M^{-1}s^{-1}$)**	
Ampicillin	405.3	691.9	1707 x 10^3	1
Nitrocefin	95.2	987.6	10373 x 10^3	1
Imipenem	13	4.8	370 x 10^3	1

3.1.6 Size-exclusion chromatography of OXA-48 mutant R206A

Size-exclusion chromatography was run on the OXA-48 R206A mutant to determine the effect of the mutation on the dimerization of the protein. The size of the OXA-48 R206A mutant as a monomer and a dimer, as well as the sizes of the three proteins used as standards is listed in table 3.12.

The chromatogram from the column ran with the three standard proteins (figure 3.22, a) only contains two peaks at 83 mL and 90 mL. It is assumed that the peak at 83 mL contains conalbumin, and the peak at 90 mL contains carbonic anhydrase. The HiLoad 16/600 Superdex 75 pg is designed to separate molecules with a molecular weight between 3 and 70 kDa, so this could explain why there was no visible peak for the aldolase standard protein, which is 158 kDa. The gel filtration of OXA-48 R206A with both high salt and low salt resulted in a single peak at 85.5 mL, as shown in figure 3.22, b. This is at a lower elution volume than carbonic anhydrase, indicating that the OXA-48 R206A mutant was eluted as a dimer. In addition, if the R206A mutant did exist as a monomer, it would not have been expected of 100% of the sample, and the size exclusion chromatography would have resulted in peaks at two different elution volumes, one for the dimer and one for the monomer.

Table 3.12: The size of the OXA-48 R206A mutant as a monomer and a dimer, as well as the sizes of the three proteins used as standards.

Construct	**Size (kDa)**
OXA-48 R206A monomer	28
OXA-48 R206A dimer	56
Carbonic anhydrase	29
Conalbumin	75
Aldolase	158

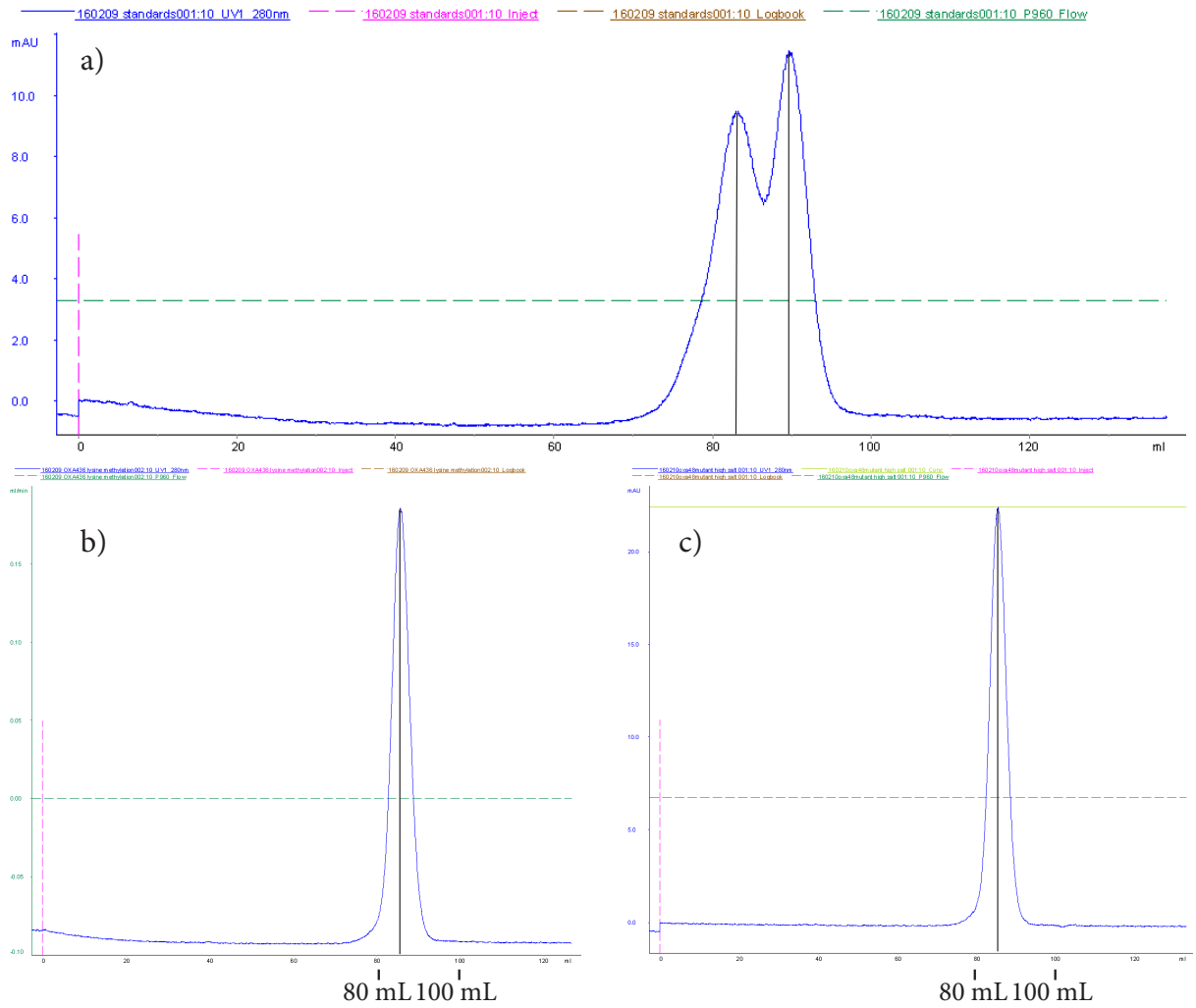

Figure 3.22: Chromatograms from the standard columns ran with carbonic anhydrase, conalbumin and aldolase (a), the column ran with OXA-48 R206A in low salt conditions (b) and the column ran with OXA-48 R206A in high salt conditions (c). **a)** The peaks in the chromatogram for the standard samples is at 83 and 90 mL. **b)** The peak in the chromatogram is at 85.5 mL. **c)** The peak in the chromatogram is at 85.5 mL.

4. Discussion

4.1 The β-lactamase enzymes OXA-23 and OXA-24

4.1.1 Restriction-free cloning of His-tagged and native *bla*$_{OXA-23}$ and *bla*$_{OXA-24}$

Amplification of bla$_{OXA-23}$ and bla$_{OXA-24}$ MPs

According to the gel electrophoresis results (figure 3.1) and the DNA concentration measurements, the amplification of the His-tagged and native *bla*$_{OXA}$ MPs seemed to have been successful. The double binding of the R1 primers for the native and His-tagged *bla*$_{OXA-24}$ constructs was negated by separating the two gene products on a gel, and cutting out the correct one.

Challenges with cloning of the His-tagged bla$_{OXA}$ constructs

Both the His-tagged *bla*$_{OXA}$ constructs proved challenging to clone successfully. In the gel results after the EMP reaction, both the His-tagged constructs showed on the gel, but the bands were very weak compared to the bands for the native *bla*$_{OXA}$ constructs. The gel results from the amplicon screening after transformation to *E. coli* XL1-blue cells did not show bands for either of the His-tagged *bla*$_{OXA}$ constructs, and only the His-tagged *bla*$_{OXA-23}$ construct was purified and sequenced.

The PCR reaction with the TEV-site MP, where the His-tagged MPs are elongated by 21 bps, was not analyzed by gel electrophoresis, as bands with a size-difference of only 21 bps would not have been separated on the gel. So the result of the reaction was not verified immediately. However, the TEV-site MP used in this reaction can possibly account for the error later observed in the sequencing of the His-tagged *bla*$_{OXA-23}$ construct; the duplicated region in the sequenced gene (figure 3.4) matches exactly with the 21 bp long region of the TEV-site MP that is constructed to elongate the His-tagged *bla*$_{OXA-23}$ MP at the 5'-end. How this has happened is however unclear, and the same sequence TEV-site MP have been successfully used by Ph.D. student Bjarte A. Lund in previous cloning protocols.

The same duplication can have occurred in the His-tagged *bla*$_{OXA-24}$ construct as well, but the gene was not sequenced, so this cannot be confirmed. The duplicated sequence was located in the region of the MP that overlapped with the pDEST17 vector, so if the error did occur during the insertion of TEV-site PCR, this would explain the weak bands in the gel results after the EMP reaction, where the MPs were to be inserted into the pDEST17 vector.

Cloning of the native bla$_{OXA}$ constructs

The gel results after the EMP reaction of the native *bla*$_{OXA}$ constructs yielded strong bands, as did the gel results from the amplicon screening after transformation to *E. coli* XL1-blue cells, indicating a successful cloning process. The sequencing of the native *bla*$_{OXA-24}$ construct confirmed the correct gene sequence. The sequencing of the native *bla*$_{OXA-23}$ construct was only done with the rev. T7 primer, meaning that it was only sequenced from the T7 terminator and backwards. Generally, the read-length is 700-800 bases when using a 50 cm capillary running on an ABI 3130x Genetic Analyzer, but this depends on DNA concentration, purity and base composition [62]. In this case, the native *bla*$_{OXA-23}$ gene was only confirmed from base 139 to the end of the gene, because of a too short read-length. If the fwd. T7 primer had been used as well, the gene would have been read both ways, and in that way all bases had been covered even with a short read-length.

4.1.2 Protein expression of native and His-tagged OXA-23 and native OXA-24

Protein expression attempts of native and His-tagged OXA-23

Expression screening of native and His-tagged OXA-23 was done in four different *E. coli* cell lines: Arctic Express, Rosetta2(DE3)plysS, BL21(DE3)plysS and BL21(DE3)pRare, but with negative results with respect to large-scale protein expression. Using the Rare Codon Calculator (RaCC) server at NIH MBI [64], several rare codons for the OXA-23 gene was reported when expressed in *E. coli.* Rare codons are defined as codons used by *E. coli* at a frequency of less than 1% [65]; during protein synthesis this may lead to depletion of the low-abundance tRNAs in the *E. coli* expression host, which again leads to poor expression of the target protein [66]. A potential solution to this codon bias is to optimize the codons in the bla_{OXA-23} gene for expression in *E. coli,* through the use of a synthetic gene where the problematic codons are replaced with codons commonly used in *E. coli.* Previous studies have reported using a custom synthesized bla_{OXA-23} gene, optimized for *E. coli* expression, resulting in a successful protein expression [27].

Protein expression attempts of native and His-tagged OXA-24

Protein expression of OXA-24 was attempted in several different volumes of both LB and TB using *E. coli* cell line BL21(DE3)pLysS as expression host, but a large scale expression of the protein was not successful. It remains unclear as to why the induction of the OXA-24 protein was so inconsistent. Induction was observed several times in 5 mL LB, but this volume is impractical for large-scale expression. In 100 mL LB, strong induction was observed once during the induction volume screening, but not in any of the ten samples of 100 mL LB during the large-scale induction attempt. Other studies have reported successful expression of an OXA-24 gene from an *A. baumannii* clinical isolate, using *E. coli* BL21 as host [35, 67].

4.2 OXA-48 mutations S118G, R206A and R250A

4.2.1 Site directed mutagenesis, protein expression and purification of OXA-48 mutants S118G, R206A and R250A

Site directed mutagenesis, transformation and sequencing of OXA-48 mutants S118G, R206A and R150A

The Phusion mutagenesis reaction, where the three mutations S118G, R206A and R250A were introduced in the bla_{OXA-48} genes, were successful for all mutations. The sequencing confirmed the correct bla_{OXA-48} sequence, with the three mutations in place.

Protein expression of OXA-48 mutants S118G, R206A and R250A

Both the small and large-scale protein expression of the OXA-48 mutants in *E. coli* cell line BL21Star(DE3)pRare resulted in induction. The SDS-PAGE analysis from the large-scale induction did not show very strong bands, but this may have been due to overloading of sample on the gel; as seen in the AFI bands in figure 3.12, the lanes look smeared and the bands are not very clear. Expression host screening was not performed, as the BL21Star(DE3)pRare cell line had previously proven effective for WT OXA-48 in experiments done by Ph.D. student Bjarte A. Lund [39].

Purification of OXA-48 mutants S118G, R206A and R250A

The SDS-PAGE analysis after purification of the three OXA-48 mutants indicated a purity of over 95% for all three mutants, which is pure enough to use in crystallization screens and enzyme kinetics studies [68]. For the S118G mutant, the purification yielded a very high amount of protein, with an end result of 173 mg. The purification of the R206A and R250A yielded 50 mg and 12 mg protein, respectively, which is enough to set up crystallization screens and do enzyme kinetics studies.

4.2.2 Protein crystallization, X-ray data collection and modelling of the three OXA-48 mutants S118G, R206A and R250A

Crystallization and crystal quality

The three mutant crystals were grown using the same conditions, and for all three mutants the conditions in row C and D (table 2.9) seemed to yield better quality crystals then row A and B conditions. This observation was based on the crystals size and shape; the crystals in row A and B were generally smaller and had a prominent needle shape, while the crystals in row C and D were larger and had a more three-dimensional structure. When stored in room temperature, relatively large crystals were obtained after only one night for all mutant screens; if the growth rate is too high, it might lead to poor crystal quality, as new protein molecules binds in a non-optimal orientation to the crystal surface [69]. The R250A mutant crystals were therefore grown on 4°C to slow the crystal growth.

Structures of OXA-48 mutants S118G, R206A and R250A

All the structure maps showed that the mutations were there. In both the S118G and R250A mutants, two new water molecules had replaced the serine and arginine residues. The S118G structure did not show bound avibactam, although the crystal had been soaked in the inhibitor. If this was a result of the mutation, it would show the importance of the S118G residue in the binding of avibactam. But, there have been some uncertainties with respect to the validity of the avibactam sample used in this experiment, as it has a different color than previously used avibactam samples.

The R206A structure was refined to the poorest resolution of the three mutants (2.61 Å), and the R_{free} value (0.28) was significantly higher than the *R*-factor (0.19). This can be evidence of an artificially low *R*-factor, and it could have been beneficial to have refined the structure to a lower resolution. But the validity of the R206A structure is supported by the S118G and R250A structures, which were both refined to fairly high resolutions with good *R*-factor and R_{free} values.

Enzyme kinetics studies on the three OXA-48 mutants S118G, R206A and R250A in comparison with the OXA-48 WT

The kinetics results for the WT OXA-48 are consistent with the expected substrate profile of the OXA-48 enzyme, and correlates well with previous enzyme kinetics studies done on OXA-48 [24]: the enzyme is reported to hydrolyze penicillins at a high level, carbapenems at a low level, and cephalosporins at very low levels that borders to no activity [20]. The WT OXA-48 in this experiment showed highest activity towards ampicillin (penicillin) followed by imipenem (carbapenem), but did not hydrolyze cefepime (cephalosporin).

The OXA-48 mutant R206A showed very similar activity levels as the WT OXA-48. The mutation is on the surface of the protein where two OXA-48 enzymes interact to form a dimer. Both the model structure and the size-exclusion chromatography results suggested that the mutation did not have an effect on the dimerization of the protein, so the mutant's similar activity profile as the WT is not surprising. If the mutation has been strong enough to break up the dimer interaction, it would have been interesting to see the effect on the enzyme activity.

The S118 residue is located in the active site of the enzyme, and interacts with the β-lactamase inhibitor avibactam through a hydrogen bond [35]. Previous studies on the class A β-lactamase enzymes KPC-2 and SHV-1 have illustrated the importance of the S118 equivalent residue S130 with respect to avibactam-inhibition; S130G mutations in the enzymes caused significant resistance to inhibition by avibactam, and the k_{cat}/K_m values against relevant carbapenems was greatly lowered when compared to the wild type enzymes [70, 71]. The activity of the S118G mutant was lowered by 60% for ampicillin and 98% for imipenem when comparing the k_{cat}/K_m values to the k_{cat}/K_m values of the WT OXA-48. This shows that the S118 residue have an important impact the OXA-48 enzyme's ability to hydrolyze β-lactams. Unfortunately, no studies were performed on the mutation's effect on avibactam-inhibition.

The R250 residue is also located in the active site of the enzyme and interacts with avibactam through a hydrogen bond. The activity of the R250A mutant was significantly lowered when compared to the WT OXA-48, with k_{cat}/K_m values for ampicillin lowered by

70% and k_{cat}/K_m values for imipenem lowered by 98%. This suggests that the R250 residue plays an important part in the activity of the OXA-48 enzyme.

Conclusion and future work

The OXA-23 and OXA-24 enzymes proved to be more difficult than expected to both clone and express. For OXA-24 the cloning difficulties were worked out by separating the correct gene construct from a shorter, incorrect gene product on an agarose gel. But in the end, we were not able to successfully express the OXA-24 enzyme. If time had allowed it, further investigations might have solved the problems and made expression of the protein possible, but as of now the reason behind the problematic expression is unknown.

The cloning of the OXA-23 enzyme resulted in a duplicated sequence around the His-tag, which might have been the reason for the weak expression. But the bla_{OXA-23} gene also contains several rare codons, so it might be necessary to optimize the gene sequence or the host in order to achieve over-expression of the protein.

The OXA-48 enzyme was successfully mutated, expressed, purified and crystallized. The enzyme kinetics studies showed that while the R206A mutant had very similar activity to the wild type OXA-48, the S118G and the R250A mutants had a significantly lower activity toward ampicillin, imipenem and nitrocefin, which again shows the importance of these residues for the overall OXA-48 enzyme activity. The S118G mutant crystal was soaked in avibactam before data collection, and the solved model did not show avibactam. But this result could be invalid, as avibactam sample used may not have been valid. In addition to doing this specific experiment once again with a valid avibactam sample, more experiments can be done here to test the effect of the mutations on the avibactam binding and inhibition.

The OXA-48 mutants described in this project will be used in collaboration between Bjarte Aarmo Lund, Hanna-Kirsti S. Leiros, Geir Isaksen and colleagues at the Brandsdalen group, with the aim of understanding the reaction mechanism of the OXA-48 using *in silico* methods. In addition, potential inhibitors are being designed in collaboration between Bjarte Aarmo Lund, Hanna-Kirsti S. Leiros and Annette Bayer's group, guided by the results of this project.

References

1. World Economic Forum, *The Global Risks Report 2016, 11th edition*. 2016.
2. Walker D., F.T., *Annual Report of the Chief Medical Officer: Volume Two, 2011: Infections and the Rise of Antimicrobial Resistance* 2011, Department of Health.
3. D/'Costa, V.M., et al., *Antibiotic resistance is ancient.* Nature, 2011. **477**(7365): p. 457-461.
4. Kolář, M., K. Urbánek, and T. Látal, *Antibiotic selective pressure and development of bacterial resistance.* International Journal of Antimicrobial Agents. **17**(5): p. 357-363.
5. Goossens, H., et al., *Outpatient antibiotic use in Europe and association with resistance: a cross-national database study.* (1474-547X (Electronic)).
6. Barlow, M., *What antimicrobial resistance has taught us about horizontal gene transfer.* (1064-3745 (Print)).
7. Wilke, M.S., A.L. Lovering, and N.C. Strynadka, *β-lactam antibiotic resistance: a current structural perspective.* Curr Opin Microbiol, 2005. **8**(5): p. 525-33.
8. Konaklieva, M.I., *Molecular Targets of β-Lactam-Based Antimicrobials: Beyond the Usual Suspects.* Antibiotics (Basel), 2014. **3**(2): p. 128-42.
9. American Chemical Society International Historic Chemical Landmarks. *Discovery and Development of Penicillin.* [cited 2016 may]; Available from: http://www.acs.org/content/acs/en/education/whatischemistry/landmarks/flemingpenicillin.html
10. Georg, G.I., *The Organic Chemistry of β-Lactams* Journal of Chemical Education, 1993. **70**(9): p. A251.
11. Blair, J.M.A., et al., *Molecular mechanisms of antibiotic resistance.* Nat Rev Micro, 2015. **13**(1): p. 42-51.
12. Essack, S.Y., *The development of β-lactam antibiotics in response to the evolution of beta-lactamases.* Pharm Res, 2001. **18**(10): p. 1391-9.
13. Rowe-Magnus, D.A. and D. Mazel, *The role of integrons in antibiotic resistance gene capture.* Int J Med Microbiol, 2002. **292**(2): p. 115-25.
14. Ambler, R.P., *The structure of β-lactamases.* Philos Trans R Soc Lond B Biol Sci, 1980. **289**(1036): p. 321-31.
15. Bush, K. and G.A. Jacoby, *Updated functional classification of β-lactamases.* Antimicrob Agents Chemother, 2010. **54**(3): p. 969-76.
16. Ghuysen, J.M., *Serine β-lactamases and penicillin-binding proteins.* Annu Rev Microbiol, 1991. **45**: p. 37-67.
17. David L. Nelson, M.M.C., *Lehninger Principles of Biochemistry*. 2008: W. H. Freeman and Company. 1158.
18. Poole, K., *Resistance to β-lactam antibiotics.* Cell Mol Life Sci, 2004. **61**(17): p. 2200-23.
19. Evans, B.A. and S.G. Amyes, *OXA β-lactamases.* Clin Microbiol Rev, 2014. **27**(2): p. 241-63.
20. Poirel, L., A. Potron, and P. Nordmann, *OXA-48-like carbapenemases: the phantom menace.* J Antimicrob Chemother, 2012. **67**(7): p. 1597-606.
21. *Align Sequences Protein BLAST* NCBI National Center for Biotechnology Information: ncbi.nlm.nih.gov.

22. Schneider, K.D., et al., *Structures of the class D carbapenemase OXA-24 from Acinetobacter baumannii in complex with doripenem.* J Mol Biol, 2011. **406**(4): p. 583-94.
23. Kaitany, K.C., et al., *Structures of the class D Carbapenemases OXA-23 and OXA-146: mechanistic basis of activity against carbapenems, extended-spectrum cephalosporins, and aztreonam.* Antimicrob Agents Chemother, 2013. **57**(10): p. 4848-55.
24. Docquier, J.D., et al., *Crystal structure of the OXA-48 β-lactamase reveals mechanistic diversity among class D carbapenemases.* Chem Biol, 2009. **16**(5): p. 540-7.
25. Walther-Rasmussen, J. and N. Hoiby, *OXA-type carbapenemases.* J Antimicrob Chemother, 2006. **57**(3): p. 373-83.
26. Poirel, L., et al., *Acinetobacter radioresistens as a Silent Source of Carbapenem Resistance for Acinetobacter spp.* Antimicrobial Agents and Chemotherapy, 2008. **52**(4): p. 1252-1256.
27. Smith, C.A., et al., *Structural basis for carbapenemase activity of the OXA-23 β-lactamase from Acinetobacter baumannii.* Chem Biol, 2013. **20**(9): p. 1107-15.
28. Bou, G., A. Oliver, and J. Martínez-Beltrán, *OXA-24, a Novel Class D β-Lactamase with Carbapenemase Activity in an Acinetobacter baumannii Clinical Strain.* Antimicrobial Agents and Chemotherapy, 2000. **44**(6): p. 1556-1561.
29. Poirel, L., et al., *Emergence of oxacillinase-mediated resistance to imipenem in Klebsiella pneumoniae.* Antimicrob Agents Chemother, 2004. **48**(1): p. 15-22.
30. Drawz, S.M. and R.A. Bonomo, *Three Decades of β-Lactamase Inhibitors.* Clinical Microbiology Reviews, 2010. **23**(1): p. 160-201.
31. Drawz, S.M., K.M. Papp-Wallace, and R.A. Bonomo, *New β-Lactamase Inhibitors: a Therapeutic Renaissance in an MDR World.* Antimicrobial Agents and Chemotherapy, 2014. **58**(4): p. 1835-1846.
32. Ehmann, D.E., et al., *Avibactam is a covalent, reversible, non-β-lactam beta-lactamase inhibitor.* Proc Natl Acad Sci U S A, 2012. **109**(29): p. 11663-8.
33. Ehmann, D.E., et al., *Kinetics of Avibactam Inhibition against Class A, C, and D β-Lactamases.* The Journal of Biological Chemistry, 2013. **288**(39): p. 27960-27971.
34. Lahiri, S.D., et al., *Molecular basis of selective inhibition and slow reversibility of avibactam against class D carbapenemases: a structure-guided study of OXA-24 and OXA-48.* ACS Chem Biol, 2015. **10**(2): p. 591-600.
35. Danel, F., et al., *Effect of divalent metal cations on the dimerization of OXA-10 and -14 class D β-lactamases from Pseudomonas aeruginosa.* Biochemistry, 2001. **40**(31): p. 9412-20.
36. Carl Branden, J.T., *Introduction to Protein Structure* 2nd ed. 1999: Garland Science, Taylor and Francis Group, LLC
37. Nelson, D.L. and M.M. Cox, *Lenhinger Principles of Biochemistry* 5th ed. 2008, New York, US. : W. H. Freeman and Company
38. Lund, B.A., H.K. Leiros, and G.E. Bjerga, *A high-throughput, restriction-free cloning and screening strategy based on ccdB-gene replacement.* Microb Cell Fact, 2014. **13**(1): p. 38.
39. Bond, S.R. and C.C. Naus, *RF-Cloning.org: an online tool for the design of restriction-free cloning projects.* Nucleic Acids Res, 2012. **40**(Web Server issue): p. W209-13.
40. Waugh, D.S., *TEV Protease FAQ*, N.C.I. Macromolecular Crystallography Laboratory, US. , Editor. 2010.

41. Petersen, T.N., et al., *SignalP 4.0: discriminating signal peptides from transmembrane regions.* Nat Methods, 2011. **8**(10): p. 785-6.
42. Macherey-Nagel, *User manual NucleoSpin® Gel and PCR Clean-up*. 2014.
43. Promega Corporation, *Wizard® Plus SV Minipreps DNA Purification System*. 2009.
44. Applied Biosystems, *BigDye® Terminator v3.1 Cycle Sequencing Kit Protocol*. 2010.
45. Zhang, Z., et al., *A greedy algorithm for aligning DNA sequences.* J Comput Biol, 2000. **7**(1-2): p. 203-14.
46. Wilkins, M.R., et al., *Protein identification and analysis tools in the ExPASy server.* Methods Mol Biol, 1999. **112**: p. 531-52.
47. Agilent Technologies. *QuikChange Primer Design* 2015 [cited 2015; Available from: http://www.genomics.agilent.com/primerDesignProgram.jsp?&_requestid=153764.
48. GE Healthcare Bio-Sciences, *Affinity Chromatography Principles and Methods*. 2007. p. 47-51.
49. Bornhorst, J.A. and J.J. Falke, *Purification of proteins using polyhistidine affinity tags.* Methods Enzymol, 2000. **326**: p. 245-54.
50. Stevens, R.C., *High-throughput protein crystallization.* Curr Opin Struct Biol, 2000. **10**(5): p. 558-63.
51. Rhodes, G., *Crystallography Made Crystal Clear* 3rd ed. Complementary Science Series 2006, Oxford, UK Elsevier Inc. .
52. McCoy, A.J., et al., *Phaser crystallographic software.* J Appl Crystallogr, 2007. **40**(Pt 4): p. 658-674.
53. Bjarte Aarmo Lund, et al., *Screening and design of inhibitor scaffolds for the antibiotic resistance enzyme OXA-48 through surface plasmon resonance screening.* Under Revision 2016.
54. Adams, P.D., et al., *PHENIX: a comprehensive Python-based system for macromolecular structure solution.* Acta Crystallogr D Biol Crystallogr, 2010. **66**(Pt 2): p. 213-21.
55. Emsley, P. and K. Cowtan, *Coot: model-building tools for molecular graphics.* Acta Crystallogr D Biol Crystallogr, 2004. **60**(Pt 12 Pt 1): p. 2126-32.
56. GraphPad Software Inc., *GraphPad Prism 7*. 2016
57. Bio-Sciences, G.H., *Size Exclusion Chromatography Principles and Methods.* 2014.
58. National Center for Biotechnology Information. *Align Sequences Nucleotide BLAST*. 2016 [cited 2016; Available from: http://blast.ncbi.nlm.nih.gov/Blast.cgi?PAGE=MegaBlast&PROGRAM=blastn&BLAST_PROGRAMS=megaBlast&PAGE_TYPE=BlastSearch&BLAST_SPEC=blast2seq&DATABASE=n/a&QUERY=&SUBJECTS=.
59. LLC, G.B. *SnapGene Viewer 2.6.2*. 2015; Available from: http://www.snapgene.com/products/snapgene_viewer/.
60. ExPASy Bioinformatics Resource Portal. *Translate tool*. 2016; Available from: http://web.expasy.org/translate/.
61. Dreyer, B., *Interpretation of sequencing electropherogram data* The DNA sequencing core facility HelseNord, Editor. 2004.
62. Online Dictionary of CRYSTALLOGRAPHY. *Free R factor* 2016 [cited 2016 may]; Available from: http://reference.iucr.org/dictionary/Free_R_factor.
63. Mura, C., *Rare Codon Calculator (RaCC)*. NIH MBI Laboratory Servers UCLA
64. Kane, J.F., *Effects of rare codon clusters on high-level expression of heterologous proteins in Escherichia coli.* Curr Opin Biotechnol, 1995. **6**(5): p. 494-500.

65. Rosano, G.L. and E.A. Ceccarelli, *Recombinant protein expression in Escherichia coli: advances and challenges.* Front Microbiol, 2014. **5**: p. 172.
66. Santillana, E., et al., *Crystal structure of the carbapenemase OXA-24 reveals insights into the mechanism of carbapenem hydrolysis.* Proc Natl Acad Sci U S A, 2007. **104**(13): p. 5354-9.
67. GE Healthcare Life Sciences, *Strategies for Protein Purification*. 2010.
68. Schmit, J.D. and K. Dill, *Growth rates of protein crystals.* J Am Chem Soc, 2012. **134**(9): p. 3934-7.
69. Papp-Wallace, K.M., et al., *Variants of β-lactamase KPC-2 that are resistant to inhibition by avibactam.* Antimicrob Agents Chemother, 2015. **59**(7): p. 3710-7.
70. Winkler, M.L., et al., *Avibactam and inhibitor-resistant SHV β-lactamases.* Antimicrob Agents Chemother, 2015. **59**(7): p. 3700-9.